Role of long-range CA3 connectivity in linking spatial and aversive information

Dissertation
zur
Erlangung des Doktorgrades (Dr. rer. nat.)
der
Mathematisch-Naturwissenschaftlichen Fakultät
der
Rheinischen Friedrich-Wilhelms-Universität Bonn

vorgelegt von
Negar Nikbakht
aus
Iran, Isfahan

Bonn, 2021

Angefertigt mit Genehmigung der Mathematisch Naturwissenschaftlichen
Fakultät der Rheinischen Friedrich Wilhelms-Universität Bonn.

Bonn, August 2021

1. Gutachter: Prof. Dr. Heinz Beck
2. Gutachter: Prof. Dr. Walter Witke

Tag der mündlichen Prüfung: November 22, 2021
Erscheinungsjahr: 2022

Role of long-range CA3 connectivity in linking spatial and aversive information

Abstract

The CA3 region of the hippocampus is an auto-associative network that is thought to enable rapid associations between spatial locations and non-spatial information. As such, it is important for retention and retrieval of contextual memories. These abilities are believed to be supported by the high degree of local interconnectivity between individual CA3 pyramidal cells via axon collaterals. This interconnectivity is also interhemispheric, with numerous dorsal CA3 pyramidal cell axons crossing the commissure and forming synapses in the contralateral CA3 and CA1 areas. In addition, CA3 pyramidal neurons also elaborate dense long-range projections that connect hippocampal areas longitudinally along the septotemporal axis. Individual axon collaterals may extend for up to 75% of the entire septotemporal axis. The role of these longitudinal axons in conveying information within the CA3 system is not well understood. The differential anatomical connectivity of ventral and dorsal hippocampus to cortical and sub-cortical areas suggests that the dorsal hippocampus is implicated preferentially in processing spatial information, while the ventral hippocampus is strongly recruited during processing of emotionally salient memories. This view, which is supported by genetic and behavioral studies, raises the question of whether the longitudinal CA3 projections are involved when animals associate spatial information with aversive or reward information.

We addressed these questions by directly imaging from CA3 pyramidal cell axons projecting from ventral to dorsal hippocampus using dual color two-photon calcium imaging in awake behaving head-fixed mice. We compared these data to measure-

ments from CA3 axons within the dorsal CA3 system (commissurally projecting CA3 axons). The task required the mice to learn the location of an aversive stimulus on a 150 cm linear track. Activity in the two axonal systems was examined in separate batches of mice while the animals encoded the space, learnt the aversive stimulus location and retrieved its memory. Importantly, we were able to track axons across multiple days of experiments to determine how their representations change during learning.

We observed that –- as previously suggested – the dorsal CA3 commissural axons showed a more precise representation of the space compared to the longitudinal, ventral-to-dorsal axonal system. During spatial aversive learning, spatial representations changed in the ventral-to-dorsal axons, with an over-representation of the linear track segment preceding the aversive stimulus present during memory formation and maintenance. This over-representation was due to a precise sequence of spatially selective stabilization and *de novo* formation of place axons. In contrast, dorsal CA3 commissural axons did not show a significant deformation of spatial maps. However, in this axon system, *de novo* formation of place axons was significantly increased in the memory maintenance phase. We show this increase to be spatially selective. Thus, ventral CA3 exhibits a defined sequence of changes in spatial coding throughout learning that precedes changes in dorsal CA3. This is consistent with a model in which the ventral to dorsal CA3 projection is relevant in the integration of aversive information into dorsal hippocampal spatial maps.

Contents

Listing of figures

As long as our brain is a mystery, the universe, the reflection of the structure of the brain, will also be a mystery.

Santiago Ramón y Cajal

1 Introduction

Learning and memory are among the most important mechanisms through which the environment influences animal behavior. Learning is the process of acquisition of knowledge about the world, while memory is the process by which that knowledge is encoded, stored and later-on retrieved to guide behavior. Many animals are born with a fascinating battery of innate behaviors, however, soon after birth many skills essential for survival have to be learned: the genome simply does not have enough capacity to contain all information needed to guide adaptive behavior. Although it is not trivial to draw a distinctive line between innate and learned behavior, we can say that for us humans, our immense capability to learn, makes us who we are because of what we learn and remember [65]. Although not all learning is beneficial (e.g., learning of dysfunctional behavior like addiction), many forms of learning are essential for survival.

For example, for an intelligent organism to survive, it is fundamental to remember the rewarding or aversive situations: where is food or the nest,

where was a predator spotted last? In associative learning, forming a memory usually requires linking multiple channels of sensory precepts to environmental cues. The animal has to be able to form a memory, but also retrieve it later on.

Thorndike's 'Law of Effect', summarizes the most pervasive form of learning across animals, reinforcement learning: "responses that produce a satisfying effect in a particular situation become more likely to occur again in that situation, and responses that produce a discomforting effect become less likely to occur again in that situation" [139]. The brain has evolved multiple solutions for reinforcement learning. One solution is to form a cognitive map of the environment, which can be referred to, in order to predict future rewarding or threatening situations. Another suggested solution is learning by trial and error [127, 140, 131] or learning a predictive map that presents each state with regard to its successor [32, 134]. In the mammalian brain in particular, the hippocampal formation (which includes the hippocampus proper, the subiculum, and the dentate gyrus) is a major hub for learning and memory.

In this chapter I will first provide a summary of hippocampal anatomy and function. Since the focus of this dissertation is on the CA3 sub-region of the hippocampus, a more detailed overview of CA3 afferent and efferent connectivity along the longitudinal hippocampal axis is then explained. Later, I will discuss the functional relevance of CA3 in different levels of this axis, after which the main goals of this project will be presented.

1.1 The hippocampus

Hippocampus (HC) as a structure in the temporal lobe, is phylogenetically one of the oldest parts of the brain and the second oldest part of the telencephalon after the olfactory system [126, 27]. In contrast to the six-layered neocortex, HC has three layers and is comprised of two main subdivisions: Dentate Gyrus (DG) and Cornu Ammonis (CA)[126]. The DG is comprised of fascia dentata and the hilus. The CA is structurally and functionally divided into CA1, CA2 and CA3. These sub-regions act

as distinct processing modules which are connected to one another serially but each has its own individual direct connections to the cortical and subcortical areas such as entorhinal cortex (EC)[19]. Inside the sub-regions, there are anatomical layers formed by the arrangement of principal cells of each region [7]. In the HC, the basal dendrites of principal pyramidal cells are in the stratum oriens (SO), pyramidal somata are in the stratum pyramidale (SP) and the apical dendrites are in the stratum radiutum (SR) and the stratum lacunosum moleculare (SLM). In the DG, between the principal granule cell (GC) layer and the hippocampal fissure, there is a molecular layer. The two blades of GCs surround the polymorphic layer, also known as hilar region of the DG. The hilar region is composed of hilar cells andinterneurons[133][fig.1.1.1]. Lesion studies in both human and rodent HC have delineated an important role for HC in episodic memory formation [21]. Episodic memory is the ability of a memory system in encoding and retrieving the order of events in unique experiences [142]. It has been reported that the disruption of the hippocampal circuitry in combination with the EC is associated with loss of short and long-term memories [126]. Although this role of the HC is quite established in the literature, neuroimaging studies have implicated the HC in emotional behavior, and provided evidence for a connection between hippocampal dysfunction and mood and anxiety disorders[67].

A look at the 3D structure of HC (vs. the more commonly investigated lamellar structure), suggests differential afferent and efferent connectivity at different anatomical levels of HC. It is therefore important to know the details of projections into these different anatomical levels. It is also important to know the role they play in communicating to different parts of the HC. Here, our focus is on the data obtained mostly from the study of rodents.

1.2 Septo-temporal hippocampus

The rodent HC extends from the cranial-dorsal to the ventrolateral position towards the caudal part where it eventually reaches the ventral surface

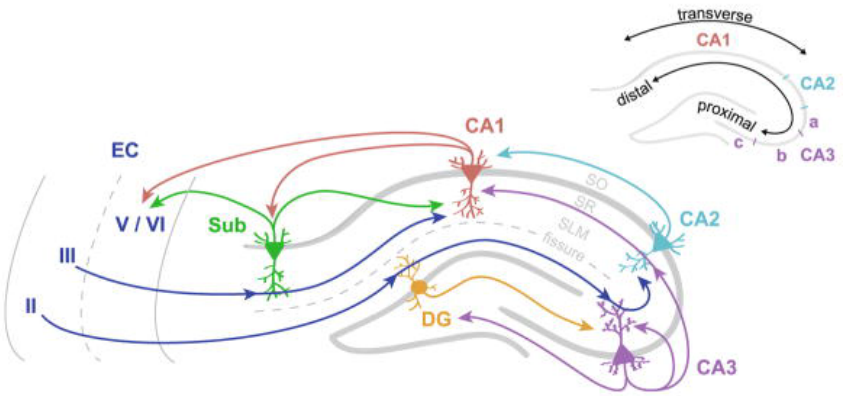

Figure 1.1.1: The hippocampal circuit - Major intra - and extra-hippocampal projections to the HC (dorsal). EC projections mainly enervate distal apical dendrites of CA1, CA2, and CA3 neurons in SLM, whereas CA3 targets the proximal apical dendrites of CA2 and CA1 neurons in SR. Arrows indicate synapses, but are not weighted by strength. Dashed grey lines indicate a subset of layer boundaries, including the hippocampal fissure and the boundary between EC layers II/III and V/VI. The depiction of the EC immediately next to the subiculum is for simplification and is not anatomically accurate; note that this exact geometry is only preserved in the horizontal plane of the ventral HC. Inset: the transverse and proximodistal axes of the HC. Also shown are approximate subdivisions of CA3 a, b, and c. Adopted from [133].

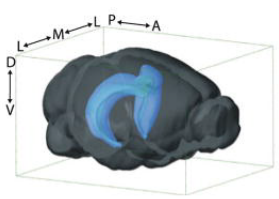

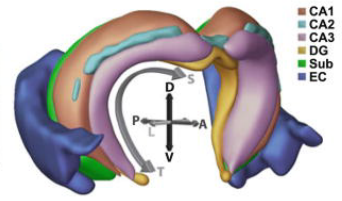

Figure 1.2.1: Upper image: relative site of the HC in the mouse brain - D dorsal, V ventral, A anterior, P posterior, M medial, L lateral. Lower image: Three-dimensional organization of the HC and EC. The hippocampal sub-regions are arranged in a way that the DG is nested most medially, and the EC embraces the temporal extent (ventroposterior) of the HC. The gray curved arrow delineates the septotemporal axis The transverse axis is perpendicular to the septotemporal axis[133].

of the brain [126][fig. 1.2.1]. In other words, it follows a dorsal (septal) to ventral (temporal) axis corresponding to the anterior-posterior axis in the human brain. Although the general anatomical organization of hippocampal sub-regions and layers inside the sub-regions repeats along this axis, due to the different cortical and sub-cortical connectivity of the HC septotemporally, functional uniformity of the HC has always been a question. In studies on dorsal and ventral HC, it has been suggested that the ventral HC is involved mostly in mediating emotional responses. This proposal is backed bythe existence of dense ventral HC connectivity to regions like, amygdala [146], hypothalamic endocrine and autonomic nuclei. Further evidence includes the selective role of ventral hippocampus in the endocrine stress response [55], as opposed to the dorsal portion of the HC which is involved in cognitive functions such as spatial memory.

This view suggests a dichotomy but rather in reality along the dorsoventral axis, there is a gradient of functional and anatomical disparity. Con-

sistent with this, gene expression studies reveal multiple functional units within dorsal and ventral portions of the HC [138]. A good example is the projections of cingulate cortex to the HC. Cingulate areas involved in emotional processing (i.e., infralimbic and prelimbic cortices), project to the more ventral regions, and cingulate areas involved in the spatial processing (i.e., retrosplenial cortex) project to the more dorsal regions in a continuous rather than discretized manner. This is also the case with projections from and to sub-cortical areas. Projections of the dorsal half of the HC innervate a small dorsal area of lateral septum (LS) and gradually more ventral areas of LS are occupied by more ventral HC projections [115]. Similarly, hippocampal connectivity to nucleus accumbens (NAc) and amygdala has progressively more projections from the ventral portions to the medial parts of these two areas [70].

Although the extrinsic hippocampal connectivity seems to follow a smooth transition along its long axis, the intrinsic circuitry, at least in rats, shows abrupt changes in some cases. For example, the longitudinal axon collaterals of CA3 pyramidal cells which are a major longitudinal association fiber system inside the HC, show extensive axonal divergence within the dorsal two-third and ventral one-third of the HC. A few axons pass between these two regions. The same applies to the DG mossy fibers axon divergence [7] and there are limited interconnections between these two sections. In rats the theta wave coherence is shown to be relatively high between the dorsal and intermediate sites but substantially lower within the ventral sites. Anatomical studies that relate this loss of coherence in line with changes in the physiology are still missing. [44].

Therefore, there is evidence of multiple longitudinal domains inside the HC, both the ones with gradual changes and the ones with sharp demarcated domains, supported by anatomical, as well as transcriptomics data. With this summary, I will focus on two major functional implications along the longitudinal axis: The spatial and the emotional coding.

1.2.1 Spatial coding along the longitudinal axis

In 1971, O'Keefe and Dostrovsky, reported that a subset of hippocampal neurons fired when rats occupied specific locations in an environment [101]. These spatially tuned neurons that were mostly recorded in the dorsal portion of the HC became famous as *"place cells"*. Place cells are ubiquitous to all sub-regions of the HC [64, 102]. Rats with dorsal HC lesions showed deficit in navigation-based memory tasks [95]. Studies as such built the bases for O'Keefe and Nadel's proposal of HC constituting a cognitive map of space [102].

Initial experimental evidence suggested that relatively small segments of the dorsal HC – a quarter or less of total hippocampal volume – is sufficient to encode spatial memory [1]. However, in a normal HC an entire two-third (almost 70%) of the HC (which also includes the ventral portion) is needed for retrieval, suggesting that rodents engage an extensive network for spatial coding [96].

[1] Lesion studies showed that a local cluster of place cells in the rodent dorsal HC is enough to form a spatial representation of the entire environment [96]

As for the ventral HC, it was shown that it encompasses a markedly lower number of place-coding cells with lesser precision [63]. A number of studies showed the size of place fields from the dorsal CA3 to ventral has a linear increase from 1m to almost 10m [71], meaning that the ventral HC might sub-serve similar roles as its dorsal part but in a larger spatial scale.

1.2.2 Emotional encoding along the longitudinal axis

The reciprocal connectivity of HC to amygdala and the CA1-subiculum is largely limited to the ventral two-thirds of the HC. However, only the very dorsal portion is void of any projection to or from amygdala [70]. An early study by Kjelstrup et al. 2002 showed that ventral but not dorsal HC was involved in defensive fear responses in an elevated plus-maze (an unconditioned threatening environment) and lesioning amygdala did not affect the defensive response in the ventral HC which might hint at, ventral HC producing the unconditioned fear response independent of amygdala [72]. The distinction between the effect of lesions on the dorsal two-third and the ventral one-third for unconditioned fear responses is pretty strong,

in that the lesions of the dorsal part have almost no effect on the fear expression but small lesions on the ventral portion do [2][72].

The connection with the NAc can also explain the role of ventral HC in reward and goal-directed behavior in rodents [123]. With regard to the intermediate HC - where the accurate place-coding of the dorsal portion meets connections to behavioral control areas in the ventral - lesion studies showed that this area is involved in rapid place learning and incorporating this learning in spatial navigation [10].

New genetic techniques and tools (e.g., CA3 region specific transgenic mice combined with viral transduction) provide a better opportunity to investigate and manipulate specific sub-regions in different levels of hippocampal longitudinal axis, perhaps in a better controlled manner compared to lesion studies. Furthermore, gaining knowledge about the genetic and molecular properties of different levels and domains of the HC along the longitudinal axis, allows targeted access to specific regions in specific levels (e.g., transgenic animals for ventral two-third of a specific sub-region like CA1). This results into further understating of relevant regions for specific behavioral implications [135].

In the present work, we focus on the CA3 region. Although septotemporal region-specific CA3 transgenic mice are not available, we utilized a CA3 pyramidal cell specific mouse-line to investigate some aspects of the hippocampal function that might manifest along the longitudinal axis. Before that, in the following sections, a general introduction about the CA3 area and its input-output pattern is presented.

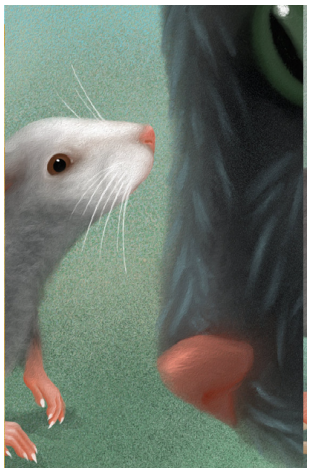

[2] Having bigger spatial fields in the ventral HC might have an evolutionary advantage, in that, the danger might be predicted and avoided from a larger distance via direct projections to the fear processing centers in the brain [135] - Image adopted and modified from J. Kuhl/Max Planck Institute of Neurobiology.

1.3 CA3

CA3 is one of the regions of the HC that has attracted special attention because of its role in memory, susceptibility to seizures and neurodegeneration. Complex and rich internal connectivity, with axon collaterals that ramify extensively and synapse onto the neighboring excitatory and inhibitory neurons creates a network that is capable of generating coherent population synchronies like gamma[3], theta and sharp-wave ripples

[3] Gamma oscillations (~25–100 Hz) are activity patterns that are found almost across all mammalian brain structures, unlike theta and SWRs that are mostly inside the HC.

[4] Theta rhythm is a prominent 4–10 Hz oscillation in the hippocampal local field potential. In rodents, they are dominant during preparatory behaviors, like ambulation, exploration, rearing and sniffing. SWRs are the most synchronous population pattern in the mammalian brain. They spread on a wide area of the cortex and are mostly occurring during periods of immobility and sleep [22].

(SWR) [4] to likely associate the firing of selected cell assemblies for special behavioral conditions [24, 27].

Despite the postulated prominent role of CA3 in computation, few studies have invested in the specifics of this region in behaving animals. In most of these studies, units recorded from CA1 to CA3 fields are reported to have very similar behavioral correlates and are analyzed together as a single group [30, 93, 97, 103, 102]. In those studies, it was suggested that CA3 is involved in spatial representations [102] and episodic memory [147].

1.4 Anatomy and connectivity of CA3

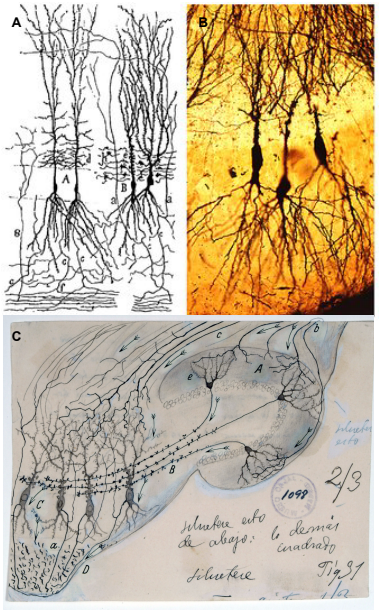

Figure 1.4.1: A and C, Early drawings of CA3 by Ramony Cajal. The presence of thorny excrescences. **B**, Original golgi-stained specimens of CA3 by Cajal. Adapted from the Cajal Institute, Spanish National Research Council or CSIC© and [86].

Inside the HC, in general, the major neuronal type and consequently CA3 area is pyramidal cells. Pyramidal cells comprise almost 191,000 cells of young murine hippocampal CA3. CA3 pyramidal cells are slightly bigger than GCs (~20 μm diameter) [16]. Li et al. 1994, reported that the total length of a projected axon of a single CA3 pyramidal neuron ranges between 150 mm to 300 mm. Based on the length and the density of boutons they speculated that a single CA3 neuron can make synapses on 30,000 to 60,000 neurons in the ipsilateral HC (mean inter-bouton distance: 4.7 μm) [85].

The dendritic trees of pyramidal cells have a basal and apical tuft. The basal tuft extends into striatum oriens (SO) and the apical tuft into the hippocampal fissure [151, 143]. CA3 pyramidal dendritic post-synapses are unique because of having structures called thorny excrescence, a feature which is also observed in some hilar cells [fig. 1.4.1] [76]. The length and organization of dendritic tree of these cells are quiet different along the transverse axis [61]. More ventrally positioned cells have an increased dendritic length in comparison with dorsally positioned ones [143]. More ventral pyramidal cells, having the largest dendritic tree also possess larger axonal trees. However, this does not hold true everywhere in the HC.

The CA3 along the transverse axis is divided into sub-divisions a,b and c [fig. 1.1.1, inset]. Sub-division 'c' being proximal to DG's hilar region and

'a' distal with regard to DG. What makes CA3 specially interesting is the highly interconnected network that this region possesses.

The following is a summary of projections within, to and from CA3 region.

1.4.1 CA3 to CA3 collateral projections

A strong CA3 to CA3 local connectivity (associational connections) is a characteristic feature of the CA3 area. This projection was the main building block of the well-established concept of autoassociative networks in CA3. This is to be taken into account that only parts of CA3 represent the autoassociative connectivity while for the other parts this feature of CA3 has to be considered in relation with input, output structures [151]. CA3-CA3 associational fibers mostly form asymmetrical excitatory synapses to interneurons in the same layer [149]. They also provide excitatory collaterals to CA3 pyramidal cells [5]. Density and extent of local connectivity is inversely related to the positioning of the pyramidal cells in the proximodistal axis [for the axis check fig. 1.1.1]. The pyramidal cells close to the hilus and within the DG do not seem to have so much local associative connectivity. Their axons stay restricted in both proximodistal as well as dorsoventral (longitudinal) axis. Further away from the DG, associational connectivity seem to increase. In one study it was shown that any CA3 pyramidal cell preferentially targets a different longitudinal stripe that is hundred microns dorsal or ventral to its cell body [85]. Where radially the axons of pyramidal cells project also seem to depend on their proximodistal position of the cell body, with more distal cells projecting to SO whereas the axons of more proximal cells project to SR [85]. Finally, position of the pyramidal cells on transverse axis also influences where the axons would terminate longitudinally. Proximal CA3 cells project to the levels anterior (dorsal) to the level of the cell, the middle portion projects equally dorsal and ventral and the distal part projects rather more ventrally [60]. The experiments related to these results however, have been mostly performed in rats, the architectural structure of dendritic and axonic pro-

[5] An axon often develops distal side branches to send the information to multiple other target neurons. These side branches are called *collaterals*. The collateral branches also modulate and regulate the neuron's firing patterns and act as feed-back system for the neural activity [116].

jections is highly species dependent.

1.4.2 CA3 to CA1 projections (Schaffer collaterals)

As mentioned earlier CA3 cells project to SO and SR of CA1 and almost entirely spare the pyramidal cell layer. Notably, the dorsoventral extent of CA3 to CA1 projection is larger than that of corresponding associative fibers. There is, however, a relationship between the transverse location of CA3 cells and the extent of their projections in CA1. Proximal CA3 projections innervate more distally in CA1 and more distal CA3 cells project to proximal positions in CA1. Also proximally originating cells end up more superficially in SO and SR compared to the distal cells. Other studies point out that most of the CA3 to CA1 connections are *'en passant'* [132, 128] and individual CA3 cells preferentially single out CA1 cells as their target and have a tendency to densely synapse in one area of CA1. It is worth noting that these findings are results of few old tracing studies which could have issues of inefficient labeling and incomplete axonal filling [85]. Proximal CA3 neurons at ventral levels seem to contribute less to the Schaffer collaterals to CA1 but, in contrast, project densely to dentate hilus and inner molecular layers of the DG [85].

1.4.3 CA3 contralateral projections

The two mentioned projections, Schaffer collateral and associational fibers, are not the only connections existing inside the CA3 area. A major input to CA3 originates from contralateral CA3. In rat, CA3 pyramidal cells project to both contralateral CA3 and CA1 and form the so called commissural projections. We also observed similar phenomenon in our virally labeled CA3 pyramidal cells.

Although commissural fiber connectivity is not investigated in detail, the few existing studies showed it to be an image of the ipsilateral organization for both the projections to CA3 as to CA1[136]. Also, the synaptic organization of ipsilateral and commissural projections is very similar, with the majority of synapses being excitatory and terminating both on pyrami-

dal cells [148, 9] and interneurons [45] (guinea pig studies). The presence of commissural fiber connectivity and its topographical organization is species dependant [6, 33] (monkey studies). Furthermore, CA3 connectivity is not homogeneous throughout the septotemporal axis, however, this architectural heterogeneity is more subtle compared to subiculum and CA1 [149].

1.4.4 CA3 and dentate gyrus connectivity

Mossy fibers, the axons of dentate granule cells (GC), send their axons to the proximal CA3 region and form *en passant* synapses [113, 14, 46, 4]. These synapses are unique in anatomy, size and their postsynaptic target structures (thorny excrescences) [fig. 1.4.1]. It has been shown that a single mossy fiber can synapse onto tens of CA3 pyramidal cell dendrites and a single CA3 pyramidal cell receives as many as 72 convergence of GC fibers [2]. There is also evidence that thin collaterals originate from parent mossy axons or terminals and terminate on cells other than CA3 pyramidal cells, i.e, local circuit neurons [28]. The connection of mossy fibers with principal or mossy cells is with large boutons (5–8 μm) while those with interneurons are targeted by smaller filopodial extensions. The mossy fiber pathway functions as a high-pass filter that translates densely coded cortical signals into a sparse, specific hippocampal code which is fundamental for memory formation [27].

However, the effect of GCs of DG on CA3 region is very much dependent on the position of GCs on the transverse axis [28]. This suggests that inputs originating from different parts of DG exert differential influences along the CA3 cell's dendritic tree and may also innervate selective groups of CA3 cells.

The extent of mossy fiber spread in the longitudinal level does not exceed a few microns (400-500 μm) from the level of original cell body [14, 28]. There is, however, growing evidence that in the distal portion of CA3, mossy fibers suddenly start leaving the transverse axis and change their direction to the longitudinal level.

The longitudinal extent of mossy fiber spread depends on the origin of the cells. The more dorsal cells could spread ventrally but the more ventral the GC body, the less the extent of longitudinal spread will be [136]. Based on the mossy fiber organization, it is wrong to conclude that the architecture of CA3 wiring is homogeneous throughout HC.

Unlike the popular view of unidirectional connectivity within the HC, there is a large body of evidence regarding CA3 back-projections to DG. As explained earlier, GCs of DG project both to pyramidal cells and interneurons of CA3 but also in the most proximal region of the CA3 pyramidal cells send collaterals that reach to the hilar region [60, 20, 85, 125]. This innervation is denser at more ventral levels of CA3. The CA3 pyramidal cells innervate not only the hilus, but also the inner portions of inner molecular levels of DG [85]. This denser collateral projection in ventral CA3, is thought to be one reason for which ventral HC is more seizure prone in epilepsy. However, the general functional relevance is not yet known.

1.4.5 Entorhinal cortex connections to CA3

Entorhinal cortex (EC) is the second largest cortical input into CA3 (septal complex is the first). This projection has been investigated in several species, including rat, mouse, monkey, cat, rabbit and guinea pig [153, 157, 34, 145].

The existence of projections from EC to CA3 and the layer of origin of these projections is thought to be species dependent. It was shown that unlike species like rats and guinea pigs, in mice, the neurons of layer II of EC project only to DG and not CA3. The detailed distribution pattern of EC-CA3 is not well investigated, although in anatomical studies of perforant pathway, projection to CA3 is mentioned [150]. In few studies in which this projection is investigated the distribution pattern seems to be similar to that of layer II of EC to DG [153]. Projections from lateral EC terminate on the outer half of SLM of CA3 while the projections from the medial EC terminate deep in the lateral fibers of CA3. The synaptic organization is also similar to that of DG and much of the excitatory EC input

terminates on the spines of dendrites of pyramidal cells and a much smaller percentage ends on the interneurons (monkey studies) [152]. It has been reported that CA3 cells in the most proximal portion of CA3 are almost entirely devoid of EC input, since their dendrites do not reach to the terminal portion of CA3 [150].

1.4.6 CA1 to CA3 projections

There are reports of back-projections from CA1 to CA3, but in contrast to CA3 back-projections to DG, these projections arise from GABAergic neurons in CA1 [130]. These GABAergic projections are most likely part of a larger GABAergic system that effects a large portion of the HC [51].

1.4.7 CA3 connections to other cortical and sub-cortical regions

The main subcortical connection of CA3 is with the septal complex.

CA3 receives inputs from medial septum (MS) and vertical limb of diagonal band of Broca and sends projections to lateral septum [5, 47, 158]. The nature of these inputs are cholinergic, noncholinergic and most likely GABAergic [5, 75]. These projections innervate the HC bilaterally and end up mostly in SO and to a lesser extent in SR and SLM. The GABAergic projection targets the GABAergic neurons in CA3 and some of these interneurons express somatostatin as well [43, 156, 50]. Most of the projections are cholinergic. In fact any alterations of MS, which in turn influences this major cholinergic input to HC disrupts acquisition [53].

It was shown that blocking CA3 cholinergic receptor with scopalamin [6] disrupts the acquisition of Hebb-William maze [117], spatial context fear-conditioning [118] and spatial novelty detection [59].

With regard to topographical organization of the septal input, lateral to medial portion of septum follows a ventral to dorsal input pattern. Same is the input pattern medial septum has for other parts of the HC. The interneuron projection most likely follows a similar input pattern [5].

It is now quite established that the only notable projection from CA3 to subcortex is to the lateral septum, which is a bilateral projection. The fibers

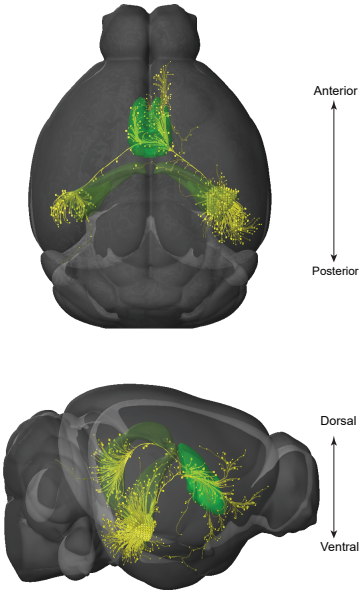

Figure 1.4.2: Projections from CA3 to the septal complex - Image copyright Allen Institute for Brain Science, https://connectivity.brain-map.org/, using Brain Explorer 2.

[6] Scopalamin (C_{17} $H_{21}NO_4$) or Hyoscine is a tropane alkaloid found in the plants of family of *Solonacea* which mimics the natural neurotransmitter acetylcholine and acts as an analouge. Scopolamine in a competitive manner can antagonize muscarinic acetylcholine receptors (mAChRs) in the central nervous system and other organs. In the body, it imposes adverse effects related to alteration of parasympathetic nervous system and cholinergic signalling and is administered because of its therapeutic effects for gastrointestinal issues such as vomiting and nausea [https://go.drugbank.com/structures/DB00747/].

of CA3 travel through fimbria and precommissural fornix and end up in the lateral septum. Some CA3 fibers cross the hemisphere and project to the equivalent level of lateral septum on the opposite side. Moreover, proximal CA3 cells project to the medial part of lateral septum while distal cells end up more lateral. Another important point is that a large percentage of CA3 cells (>75%) project both to CA1 and lateral septum [137]. There is also a report of single cell that provided collaterals to CA3, CA1, as well as lateral septum both ipsi- and contralaterally, hence three different target areas at the same time. The functional relevance of such projections is therefore, beyond the simple autoassociative network that provides input only to CA1.

Other cortical areas that communicate with CA3 are the amygdaloid complex and endopiriform nucleus [11, 107, 108] and there is also some inputs from aminergic nuclei in the brain [3]. Unlike CA1 and subiculumn, CA3 (just like DG) does not receive any thalamic input [55, 155, 129].

Rajasethupathy et al. 2015, reported a monosynaptic top down projection from prefrontal cortex to CA3 and CA1 in mice, more specifically from anterior cingulate cortex. Optogenetic manipulation of this projection helped with the retrieval of contextual memory [112].

1.5 Role of CA3 in hippocampus

In order for the hippocampus-dependant memories of events and contexts to be formed, incorporation of a complex configuration of stimuli into a memory trace is needed. These memories should be retrieved or recognized later [102]. Hippocampal sub-regions most likely serve distinct but complementary roles in the HC, e.g: CA1 is important in formation of spatial reference memory and novelty-detection, less sensitive to contextual discrimination while dentate gyrus (DG) is thought to have the ability of pattern separation at the level of output, an ability of distinguishing two very similar contexts from one another, and CA3 is thought to be involved in a process called pattern completion.

Pattern completion, as a basic property of biological memory systems, is the ability of retrieving a complete memory by means of partial sets of sensory cues. The anatomical positioning of CA3 in the HC and the extensive recurrent connectivity of CA3 cells, make this region a great candidate for pattern completion. There is evidence that memory can be retrieved in highly associative networks with modifiable synapses, the two properties that are found in CA3 region [102, 53]. Nakazawa et al. 2002, showed that knocking the gene for subunit 1 of NMDA-receptor out in a CA3- specific transgenic mouse resulted in impaired ability of the mice to retrieve the memory while presented a partial set of original cues. These mice learnt the task properly and had a normal CA1 place representation in the original but not in the cue-reduced environment, hinting at the impaired retrieval [100].

In addition to the mentioned role, from a behavioral point of view, CA3 sub-divisions are thought to play a critical role in the encoding of novel spatial information within short duration (minutes to seconds). This is easily reflected in tasks that require one trial short-term learning and working memory, rapid encoding and novelty detection. CA3 are also involved in spatial tasks that require relational associations, within the frame work of auto-associative CA3 network. In cooperation with CA1, via Schaffer collaterals, CA3 also has a role in processing sequences and lastly in connection with the DG it is mentioned that it serves a role in processing the geometry of the environment [66]. The following sections address a more in-depth explanation of some of these roles.

1.5.1 Spatial coding in CA3

One of the suggested processes for CA3 within short-term memory is rapid acquisition of novel information in the environment. This ability encompasses rapid formation of place representations in the CA3 principal cells. An ability most likely due to the modifiable synaptic strength of recurrent collateral and associative network inside this region. It was suggested that this network can act as an attractor [92, 119] which is most likely useful for

some forms of working memory [7]. In an study by Lee and Kesner 2002, injection of NMDA receptor blocker AP5 in CA3, impaired the ability of rats in performing a non-matching to sample task in a radial armed maze [8] [58, 78].

In another region-specific lesion study, the role of CA3 in rapid encoding of the novel spatial information in a contextual fear conditioning task was studied. The rats with CA3 lesions showed delayed freezing responses to the context, which suggested that the ability of lesioned animals in formation of the memory of the novel contextual cues was impaired [79]. It was also shown that on a ring track with four different cued textures, the plasticity mechanisms were only activated when the rats encountered the novel configuration of familiar cues. In this case, the local cues that were previously rotated clock-wise, in the test session were being rotated counter clock-wise and the distal cues were rotated the opposite direction [80].

A known behavior of place cells in the HC after repeated experience of an environment, is backward shifting (opposite to the running direction of the animal), a mechanism related to NMDA-dependant plasticity [39]. This shift in the mentioned ring track, after the configuration change, happened during the first encounter in the CA3, way more prominently compared to the shift in the CA1 area. This change was no more observed after two days in the CA3, while in CA1 this phenomenon happened after two days, pointing to different time courses of place-coding, in this case, in the two-areas (double dissociation). In this study by Lee et al. 2004, the authors suggested that the phenomenon they observed is due to CA3 acting as a fast incorporator of novel place information into an existing system [80].

Conversely, in a recent study, Dong and Sheffield 2020, experimented a real time, trial by trial formation of place maps in CA1 and CA3 using calcium imaging. In their time scales they found that upon exposure to a novel environment in CA1 a proportion of cells (more than 30%) instantly form place fields (PF), and these PFs, upon experience shift back and partially remap in the trials. Instant formation of PFs in CA3 only happened

[7] In general, an attractor network is a network of nodes (i.e., neurons in a biological network) that are often recurrently connected and over time evolve to a stable pattern. That pattern may be stationary, time-varying (e.g. cyclic), or even stochastic-looking (e.g., chaotic), an attractor network can generally hold only one item active during a delay period via sustained firing [http://www.scholarpedia.org/article/Attractor_network].

[8] D-2-Amino-5-phosphonopentanoic acid (AP5) is a chemical compound used as a biochemical tool to study various cellular processes. It is a selective NMDA receptor antagonist that competitively inhibits the ligand (glutamate) binding site of NMDA receptors.

in 9% of the cells. Majority of CA3 PFs were formed gradually, perhaps through spike timing dependant plasticity (STDP) and stayed significantly more stable across trials compared to CA1 PFs. These stable pyramidal cells in CA3 are the ones that are instantly reactivated upon re-exposure to the context during the following days and CA1 constantly forms a high proportion of new place cells [36]. The high reorganization of CA1 maps might hint to offline plasticity during sleep[124]. They further discuss that the fast and instant CA1 place field formation can act as an online updater in HC for rapid learning and storage of episodes of events in a single trial [81]. In CA1 a backward shifting of place field population happens during ongoing experience, this might be what allows the CA1 to gradually predict future locations in a context [88, 134]. Prediction of future by CA1 is a product of asymmetric plasticity that strengthen the synapses that are activated earlier in the context during each traversal [94]. Then, CA1 rapidly generates representations of the environment (the world) that are continuously formed by exploration to predict the future (where am I going?). Simultaneously, the CA3 generates gradual representations that are stored during experience and encode the present moment (where am I?). The stable place cells in CA3 are rapidly reinstated during re-exposure to same context, which might support memory recall [36]. In fact memory recall of spatial context is supported by the reactivation of stable PFs upon re-exposure. [38].

The apparent discrepancy in observation of the two mentioned studies regarding the CA1 and CA3 place field formation, most likely arises from their different methodology and experimental set-up. In Lee et al. 2004, the test phase included all the same spatial cues that the animal had already experienced and only the direction of cue presentation changed. It is possible that some features of the environment were encoded into the CA3 network synapses and re-exposure to the environment with the new combination of cues, quickly reactivates those potentiated synapses inside the CA3 network, this happens much faster than CA1, while in the Dong and Sheffield 2020 study animals stepped from a familiar environment into an entirely novel space. In this case, CA1 through direct input from EC and

nucleus reunion, quickly incorporates the spatial information into CA1 synapses. The comparison of stability in this study was done between the first and second half of the novel environment's experience. Therefore, the time scales differ between the two studies too.

There is evidence that learning and retrieval upon multiple trials are CA3 dependent. It was shown that an isolated CA1 area is able to encode the spatial information in the environment and form sharp PFs, most likely through direct extrahippocampal connections (e.g: EC), but is unable to retrieve these representations without CA3-CA1 communication during the following days [19]. An observation that held true in a CA3 lesion study with a multiple trial water-maze task [19]. However, as mentioned earlier, Nakazawa et al. 2002, in their study showed that CA3 specific NMDA knock-out mice learnt the water-maze task as good as the control mice, but failed to retrieve the memory in the following days [100].

In lesion studies that utilized tasks requiring multiple trials for learning like, Hebb-William maze task and object place recognition task, it was shown that CA3 is required for acquisition of the task within a day, while CA1 lesions impair retrieval across days [62, 144]. For such tasks, it seems like the CA3 output to fimbria fornix is essential, while the output to CA1 seem not to be as crucial. This observation might be due to the influence of CA3 on LS and eventually MS area via fimbria. Alteration of MS means alteration of the main cholinergic input to the HC, hence reducing the long term potentiation (LTP) in recurrent collaterals, and as a result, acquisition.

1.5.2 Encoding and retrieval of fear memory in CA3

An intelligent organism in order to survive, requires adaptive perception of the environment through which it navigates. It must be aware of the threats that might come along its way. It needs to both remember where in the context, a certain danger is, and simultaneously update its current information about that hazardous situation to be able to predict a forthcoming one.

HC is a center for contextual information processing and mediates input to areas that process the fear response. Consequently, an animal can produce appropriate response to a given dangerous condition [13]. Clearly, the appropriate evolutionary response in a threatening situation is 'fear', which triggers defensive behavior. The dorsal and ventral HC, divide the labor and mediate the adaptive fear response. In this process the dorsal HC is responsible for contextual discrimination (e.g., distinguishing old from novel), navigation and exploration (e.g., forming a spatial map)[135], while the ventral HC orchestrates goal-directed and anxiety-related behaviors [40]. Subsequently. this cooperation makes it possible to retrieve the fear memory later and links it to the location of the fearful experience as well.

As we saw in section 1.2, hippocampal CA3 as a sub-region receives a large set of different inputs along the septotemporal axis and its output is then channeled onto different target areas. Therefore, CA3 projections within HC as well as the extra-hippocampal CA3 projections, participate in different aspects of learning and behavior at different levels. Notably, even the classical CA3 to CA1 projections serve different roles depending on their anatomical positioning within the dorsoventral axis. For instance, it is thought that the information related to resolving similar contexts, communicated between dorsal DG and dorsal CA3, is sent to dorsolateral septum (DLS) via direct synaptic connections and from there relayed to other brain regions (hypothalamus and the supramammilary nucleus) [115, 104, 91]. Furthermore, Lee and Kesner 2004 showed that dorsal CA3 and CA1 lesioned animals exhibit deficit in encoding of contextual information during the contextual fear-learning task and this deficit was more prominent in dorsal CA3-lesioned animals compared to dorsal CA1-lesioned ones [79].

It was also shown that, excitotoxic lesions of dorsal CA3 and CA1 caused deficits in acquisition of contextual fear memory but lesions of dorsal CA1, ventral CA3 and ventral CA1 impaired retrieval and expression of contextual fear 24–48 hours after the encoding [58]. CA3 output projections to DLS have been shown to have an important role in contextual fear

discrimination [12]. There is evidence that the projections of dorsal CA3 to downstream DLS calibrate the responses in ambiguous contextual fear conditions while the dorsal CA3 to dorsal CA1 plays this role in certain contextual threats. Ventral CA3-DLS projections mediate fear responses in both unambiguous and ambiguous contexts in a negative manner (suppression), whereas ventral CA3-CA1 projections promote fear responses in both of these contexts [13].

It is assumed that both processes of encoding and retrieval interact on a trial-by-trial basis in any given behavioral task [66]. One powerful and advanced technique in elucidating the neural activity in awake behaving animals is *in-vivo* calcium imaging combined with trial-based behavioral tasks. The following section is a short introduction to the two-photon calcium imaging technique and our approach of utilizing it in our study.

1.6 Calcium imaging of CA3 axons

Calcium transients are a reflection of neuronal electrical activity. Influx of calcium inside a cell is associated with electrical events such as synaptic activation and dendritic spikes. Measuring concentrations of calcium ions using optical methods in cells, is called calcium imaging. Advancements in imaging techniques as well as development of genetically encoded calcium indicators (GECIs), which act as fluorescent protein sensors of Ca^{2+} and report the change in their emission amplitude or spectrum, have made high quality, high signal-to-noise-ratio measurements possible. Apart from technological advancements, since measuring synaptic activation and dendritic spikes are difficult with other measurement methods, calcium imaging comes in handy. It is noteworthy that a signal reported by a calcium indicator is the convolution of the actual calcium transient and the indicator's response [1]. Therefore the choice of Ca^{2+} indicator in interpretation of Ca^{2+} signal matters.

Except in few cases, biological tissues cause strong optical scattering, making high-resolution deep tissue imaging impossible. Linear (one-photon) near tissue microscopic techniques, such as normal confocal,

make at max. 100 μm depth of imaging, *ex-vivo* possible. Non-linear imaging techniques, on the other hand, have special properties that make them less sensitive to light scattering. Two-photon excited fluorescence laser scanning microscopy (2PLSM) combined with *in-vivo* fluorescent labeling therefore, has become a popular technique in monitoring activities of hundreds of cells [54].

In the present work, we aimed at two-photon imaging of the **axons** of CA3 pyramidal cells originating in the **ventral** or **contralateral - dorsal** CA3 through a hippocampal window. A portion of the window always covered the most rostral tip of the HC, where CA3 starts and the remaining two-third covered the top of dorsal CA1. The bottom of the window met, in depth, the Alveus. The positioning of the window is supported by studies that pointed to the fact that a single CA3 pyramidal cells arborizes most extensively in the CA1 region, covering approximately two-thirds of the longitudinal axis of the HC. It was shown that the total length of axon collaterals in the CA3 region was less than in CA1 and the axon branches tended to cluster in narrow bands (200–800 μm), usually several hundred microns anterior or posterior to the cell body [85]. However, as mentioned, with our 3mm window we had the possibility of monitoring the activity of axons terminating in both regions.

Axonal Ca^{2+} signals represent depolarization in presynapse and therefore provide information about afferent activity [1]. Long-range projection Ca^{2+} imaging has been practiced in studies of visual cortex projections to higher visual areas [48] or afferent connections to motor cortex [106].

The origin of Ca^{2+} signals at axons is membrane depolarization. Studies showed that in cortical layers 2/3, the mediation of Ca^{2+}, specially close to the synaptic active zone is through voltage-dependant Ca^{2+} channels, like P/Q and N - sub-types [29]. It has been estimated that Ca^{2+} signal in axons has a fast rise of ~1ms and decay time-constant of ~60ms. Axonal Ca^{2+} has a reliable fidelity with elicited action potentials [1].

The intensity of Ca^{2+} transients is highly variable at different axonal boutons of even the same axon (10 fold variability) [74], independent of the distance from soma [73]. Apart from the postsynaptic cells [73],

neuro-modulators such as adenosine [29] and dopamine also influence the intensity of Ca^{2+} transients at the axonal boutons. Studies on retrosplenial cortex (RSC) that sends projections to cingulate and secondary motor cortices showed that the response to electrical stimulation of RSC is a graded increase in the evoked fluorescence transients in the axonal boutons.

1.7 Head-fixed behavior and contextual fear learning

Fear memory conducts adaptive behavior in contexts associated with aversive stimuli [87]. The HC can form a neural map of the context which predicts fear. Contextual but not cue dependent fear-conditioning is believed to be HC-dependent. In the original contextual fear conditioning paradigm, typically a rodent is placed inside an arena with particular physical features and receives pairings of a phasic tone to a mild electrical footshock. When tested in the conditioned environment, the animal freezes (without the tone presentation) - a natural defensive behavior in rodents [15]. This is the so-called *contextual fear conditioning* (CFC). The animals also freeze to the tone, in a different environment from the one they were trained in, which is, *auditory-cue fear conditioning* [122]. Lesion studies provide evidence that almost in all cases, damage to the HC, be it excitotoxic or electrolytic, retrogradely impairs CFC. This is regardless of the lesion location being in the dorsal or ventral HC or bilateral in both [8, 42].

A conditioning context usually includes a set of features like, floor texture, odor, sound, particular ambient light and a particular shape and size. During CFC, brain performs two functions in series: first forming a unified multisensory representation of the conditioned environment or conditioned stimulus (CS) and then associating the CS to the aversive or unconditioned stimulus (US). It has been suggested that the encoding of independent features happens in cortical areas [98], [99] but the integration of all features of an environment into a unified concept as 'context' relies heavily on the interaction of cortex with HC [121]. In other words, the HC acts as a binder of independent sensory information from an episode as an *auto-associator*. More specifically, it has been shown that the CS is

encoded by the dorsal HC [41] and its outputs are associated through synaptic plasticity with US in amygdala [68]. With recent advancements in imaging techniques and the possibility of recording activity of cells *in-vivo* and awake preparations, head-fixed behavioral paradigms have been devised and are frequently used.

Head-fixation has been used for behavioral studies, specially in non-human primates, for accurate stimulus control, behavioral monitoring and optical or electrical neural recordings [52]. We developed a variation of head-fixed CFC (hf-CFC) that was originally described in Lovett-Barron et al. 2014. In their study, they water restricted the mice and taught them to lick water rewards while being head-fixed on a linear track. Lovett-Barron et al. 2014, then exposed the head-fixed animals to two multisensory contexts that included two different sets of auditory, odor, visual and tactile conditions. They monitored the licking activity over three consecutive days. On the day 2, they paired one of the contexts with an airpuff as the US and assessed the licking in the two contexts. They used conditioned suppression of water licking as a criterion of learning. They argue that in head-fixed condition, freezing is a poor behavioral read-out. Conditioned suppression of water licking has been used as a proxy for learning in two older studies in freely moving rats too [89, 17]. Using this read-out, they found that the licking rate was significantly reduced in the conditioned context [87].

In our version of the task, we have reduced the number of sensory information presented to the mice. Instead of the two neutral and conditioned contexts, we heavily relied on the tactile cue-rich patches on a belt and the ability of the mice to distinguish them from one another. This was similar to what was used in Lee et al. 2004 for the circular track with different textured zones [80]. After a period of baseline training, we paired a given patch with the presentation of airpuff. As behavioral read-out, we relied on the change of running speed around the location of the patch, paired with airpuff as a sign of learning (for further details see section 2.6 and fig. 2.6.2). The mice performed the task head-fixed under a two-photon microscope.

1.8 Rationale of this work and its primary objectives

In this thesis project we hypothesized that the longitudinal ventral to dorsal (V-D) axonal projections of CA3 pyramidal cells can link anxiety related ventral HC to the dorsal spatial HC. This hypothesis is supported by several lines of evidence: a) as mentioned in section 1.2.2, ventral HC is involved in emotional aspects of memory formation. b) ventral HC is densely connected to regions such as amygdala, hypothalamic endocrine and autonomic nuclei. c) intrahippocampal networks of CA3 are highly interconnected d) ventral CA3 extensively projects to the dorsal portion of the HC and e) dorsal HC plays an important role in spatial coding.

So far, very little is known about the role of intrahippocampal associational and longitudinal fibers of CA3 and consequently the clear function of such long-range projections remains unknown. In this thesis we set out to investigate the following questions:

1. What are the different functional properties of the commissural–associational (D-D) CA3 axons and longitudinal (V-D) axons?

2. What are the representational changes in these axonal systems in the course of behavior and in what way are these changes correlated to learning?

These two axonal projections, despite having different cellular origins (dorsal-contralateral CA3 and ventral-ipsilateral CA3 with regard to the imaging site), mix and terminate in similar target areas, i.e., dorsal CA1 and CA3. As such, before us, with the existing neural recording techniques it was not possible to segregate their activity in order to study their respective roles. In this project, using *in-vivo* two-photon calcium imaging and a CA3-specific transgenic mouse line, we developed techniques that enabled us to study these projections separately. We combined these recordings with an appropriate behavioral task.

2

Materials and Methods

To address the questions mentioned in the previous chapter, I, together with Martin Pofahl established the *in-vivo* two-photon Ca^{2+} imaging in the Beck lab, starting from the treadmill apparatus, implants, surgical procedures of hippocampal window implantation and the behavioral paradigm. In this chapter, I will briefly explain the technical details of our two-photon *in-vivo* imaging system in combination with a variant of contextual fear-learning paradigm and the technical and analytical procedures we utilized.

2.1 Subjects

All animal experiments were conducted in accordance with the European (2010/63/EU) and Federal law (TierSchG, TierSchVersV) on animal care and use and were approved by the county of North-Rhine Westphalia (LANUV AZ 84-02.04.2015.A524).

Mice were single caged, or in rare occasions, kept in pairs. They were maintained on a 12-hour reversed light/dark cycle (lights ON 6PM–6AM). All the experiments were conducted during the dark phase. Mice had access to food *ad libitum* before the start of the experiments and as soon as the habituation to the belt started, they were food scheduled [see section 2.6 for details].

In this study we used 6-12 week old *Et-iCre* transgenic mice. This strain was originally from Ronald L. Davis and Paul Overbeek and the primary reference is given on CRE-driver network established by the NIH Neuroscience Blueprint.

2.2 Viral transduction and head-fixation implantation

In a single operation, injection of the calcium indicator, pAAV.Syn.Flex.GCaMP6s.WPRE.SV40 (AAV1) and implantation of a customized head-fixation was performed [fig. 2.3.2 C]. The animals were subcutaneously (s.c.) injected with ketoprofen (5 mg/kg body weight) 30 minutes prior to the surgery. They were then anesthetized with a combination of fentanyl/midazolam/medetomidine (0.05 / 5.0 / 0.5 mg/kg body weight, i.p.) and were head-fixed in a stereotactic frame. Their body temperature was kept with a heat-plate at 37°C and their eyes were covered with ophthalmic ointment (Bepanthen, Bayer), in order to prevent them from drying out. The hair over the scalp was cut short, and then was cleared completely with a hair-remover cream (VEET Haarentfernungscreme). The scalp was then completely disinfected.

After the application of local anesthetics (10 % lidocaine), a pear-like circumference of skin was removed. The lidocaine was again applied and the thin, transparent remaining connective tissue under the scalp was scraped away using a scalpel. Using a dental drill, a golf-ball-pattern was made all over the skull in order to enhance the grip between the head-fixation and the dental cement. The skull was then cleaned further with a Q-tip immersed in 1 % H_2O_2. The Q-tip was robbed on the skull with care, avoiding the skin around the ears and eyes. The skull was thoroughly

washed with abundant amount of dPBS in order to get rid of any remainder of H_2O_2 and to avoid tissue necrosis. The area was air-dried and subsequently, a thin layer of the primary component of OptiBond (OptiBond™ 3FL; two component, 48 filled dental adhesive, bottle kit; Kerr; FL, USA) was applied in a circular fashion with a pipette tip. A distance of 1-2 mm from the surrounding skin was maintained. The secondary component of OptiBond was immediately applied over the primary circle, was well mixed and then cured with a UV lamp. Based on the Bregma, a small craniotomy for the injection of GCaMP6s was made using the dental drill with the following coordinates:

Dorsal CA3: AP: - 0.1; LA: + 0.1; VD: - 0.17 (fig. 2.3.2 A)

Ventral CA3: AP: - 0.3; LA: - 0.32; VD: - 0.37 (fig. 2.3.2 B)

Subsequently, the tip of NanoFil Microsyringe (NANOFIL, 10μL, cannula size 34 G, World Precision Instruments, Sarasota, FL) was navigated stereotactically through the burr hole. For the dorsal position, 250 nL GCaMP6s with the speed of 20 nL/min was injected into the brain. Similarly for the ventral CA3, 300 nL of the virus with the same speed was injected.

The position of the cranial window was marked using a 3mm biopsy punch (Kai Medical, Integra® Miltex® disposable biopsy punch 3mm). To have a stable fluorescent signal for the motion correction during the analysis, a red labeled reporter virus, rAAV 2/1-GFAP-mcherry was injected inside the marked window position. The injection was done at 3 different locations across the marked circle and in each location in two different depths:

1st inj.: AP: -0.14; LA: -0.1; VD: -0.14, -0.17

2nd inj.: AP: -0.3; LA: -0.32; VD: -0.37

3rd inj.: AP: -0.3; LA: -0.32; VD: -0.37

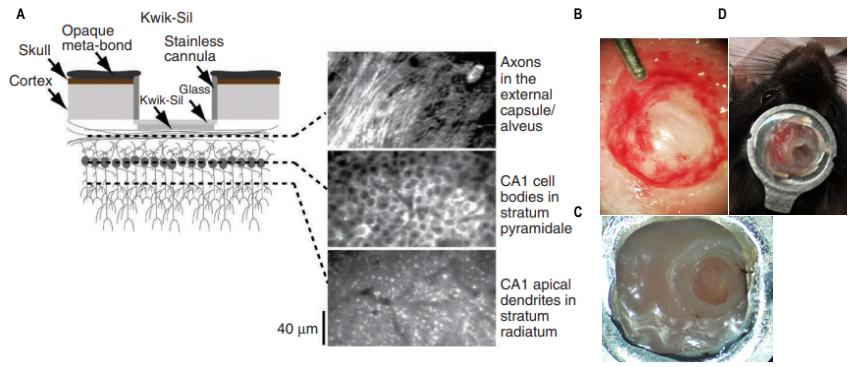

Figure 2.3.1: Detailed view of hippocampal window - A, a detailed view of the hippocampal window as it was described in Dombeck et al. 2010. For CA3 fibers we stopped the aspiration at the same level as in the Dombeck's description and imaged the labeled axons in the external capsule. **B,** the alveolar view of our example window and the external axons. **C and D,** the final look of the window with the inserted silicon block together with the head-fixation - Image in **A** adopted from [35].

A total volume of 150 nL was infused into the HP during each injection with the rate of 20 nL/min. The injection holes were covered by a thin layer of UV-cured dental cement (Tetric Evoflow). Consequently, Tetric Evoflow was applied in a circular fashion close to the marginal skin. A small amount of dental cement was also applied underneath the head-ring [fig. 2.3.2]. The head-ring was then placed on the skull and the dental cement was cured with a UV-lamp. An antibiotic ointment (Refobacin Creme, 1mg/g Gentamicin, Almira) was then applied on the skin surrounding the head-ring, and Naloxone was injected i.p. (0.1 mL/10 g body weight) to reverse the effect of anesthetics and wake the animal up. The animals were then returned to their home cage for recovery. The cages were kept on a warm-pad for few days after the surgery and a small amount of soaked food was placed on the cage's bedding for easy access. Postoperative Buprenorphine was administered once daily for three follow up days (5 mg/kg body weight, s.c.).

2.3 Craniotomy and hippocampal window implantation

The principal procedure of craniotomy was as described in Dombeck et al. 2010 [fig. 2.3.1 A].

Dexamethasone was i.p. injected (0.1 mg/20 g body weight), 45 minutes before the start of the surgery, in order to prevent brain inflammation

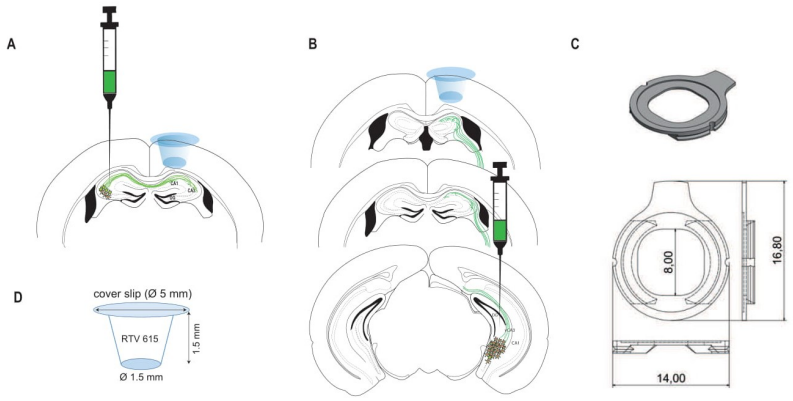

Figure 2.3.2: GCaMP6s was virally transduced into the target areas - A, Dorsal CA3 injection site, **B,** Ventral CA3 injection site, **C,** The head-ring design, **D,** The PVC silicon block used as the the insert. A cover glass of 5 mm width was attached to the top of the silicon block and held the insert over the skull.

during the surgery. The animal was anesthetized inside an induction chamber with 3-4% isoflurane mixed with an oxygen/air mixture (25/75%) and was then transferred to a stereotactic frame. An isoflurane mask was put on the snout and the head was fixed using head-bars. The anesthesia was maintained with a reduced isoflurane dose of 1-2% at a gas flow of about 0.5 l/minute. Eyes were covered with ophthalmic ointment (Bepanthen, Bayer) to prevent drying and body temperature was maintained at 37°C using a regulated heating plate (TCAT-2LV, Physitemp). The skull in the middle of head-ring was thoroughly cleaned using a Q-tip soaked in 70% ethanol. Based on the previously made circular mark on the skull, a Ø 3 mm craniotomy was made using a dental drill. The circular piece of skull was gently removed and any remaining bones around the edges were smoothed and drilled away. With a blunt needle attached to a suction system, the cortex was then carefully aspirated until the alveus of the HC [fig. 2.3.1 B], the brain was when required perfused with dPBS to prevent blood from clotting and drying of the brain. The silicon insert [fig. 2.3.2 D] was then gently placed inside the brain and rims of the window were sealed with dental cement (Tetric Evoflow) and cured with UV-light [fig. 2.3.1 C, D].

2.4 Linear track

We built a horizontal linear track [fig. 2.4.2], adapted and modified from the models in Lovett-Barron et al. 2014 and adjusted to our commercial two-photon set ups (A1 MP, Nikon, Japan). A velvet band (150 cm length and 4.5 cm width) ran on two 3D printed wheels [fig. 2.4.2] and slid on a Teflon plate. The wheels were fixed with shafts attached to 3 mm ball bearings. During the experiments, mice were kept in position under the objective with metal head-holders that clipped the ring-like head-fixation on their head [fig. 2.4.1].

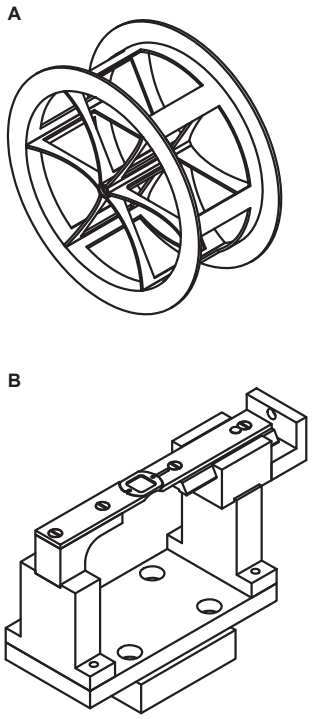

Figure 2.4.1: The design of the 3D printed wheel and the head-holder - A, the wheels were 3D printed with a 5cm width and 10 cm diameter. The material was *VeroWhite resin* . **B,** the head-holder had two movable clamps that could be fixed around the head ring with a screw. The bottom part was mounted on a lab jack for height adjustment. The belt passed through the head holder frame. Designs: Courtesy of the late **Mr. Klaus Granitza**.

To configure the right distance of the mouse's head from the belt, the head-holder was mounted on a lab-jack (L200, Thorlabs Inc. Newton, New Jersey, USA). The angle of the head-holder was made adjustable with a two-axis goniometer (GNL20M, Thorlabs Inc. Newton, New Jersey, USA). In order to encode the speed and position of the animal, an optical mouse sensor was implemented on the back wheel and was controlled by an Arduino micro-controller (Arduino Uno, Arduino AG, Italy). A reflectively sensor was additionally implemented inside the Teflon plate, close to the back wheel, for reporting the location. The back-side of the belt was marked with stripes of black teaser film to define the borders of three 50 cm zones and helped a more precise report of the animal's position. The treadmill was further equipped with piezo-speakers (Piezo speaker bricklet, Thinkerforge, GmbH, Germany) for auditory stimulus delivery, a reward delivery system attached to a peristaltic miniature Pump (RP-Q series, TakasagoFluidic Systems, Japan) and an airpuff delivery system. Airpuff delivery system was a tubing attached to the compressed air system of the lab and was controlled by a solenoid valve (Series 3-Miniature Inert Liquid Valve, Parker, USA). All the stimuli equipment and the reflectivity sensor were controlled by a Tinkerforge Master Brick micro-controller (Tinkerforge GmbH, Germany). The entire treadmill set-up was installed on a move-able sliding table (380FM-U, Luigs and Neumann, Germany). The behavioral data from the belt was collected at a frequency of 100Hz and was then down-sampled to match the imaging data. The data acquisi-

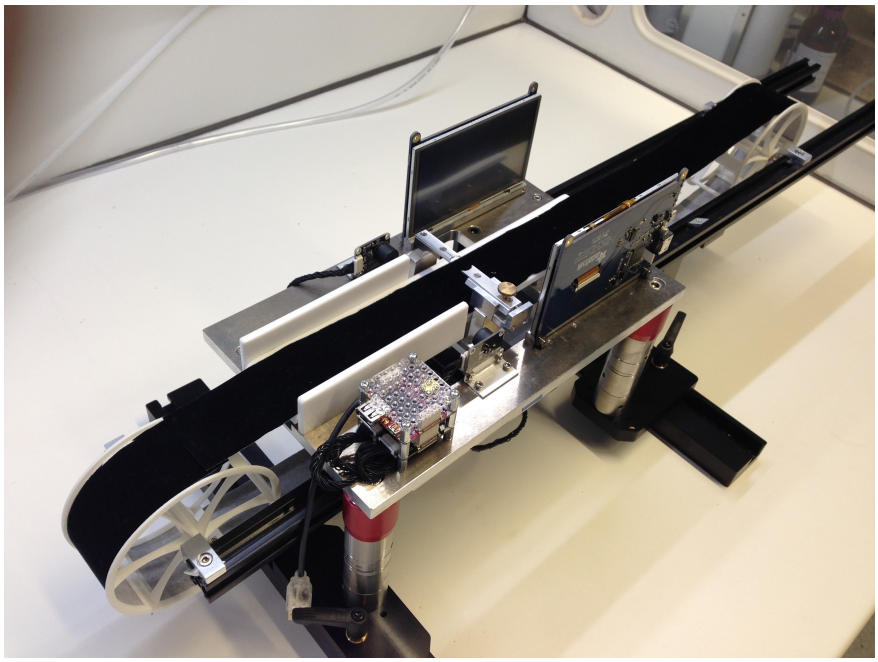

Figure 2.4.2: A prototype of the customized horizontal treadmill with the belt - The horizontal treadmill was mounted on two sliding bars, compatible to the rails under the two-photon microscope in order to be moved back and forth for convenience (the two large black bars). The bright black velvet fabric slid on a Teflon plate and two 3D printed wheels. Wheels were attached to the treadmill with shafts. A microprocessor collected the data and delivered stimulus commands.

tion and stimulation command control was made possible by a customized n LabView software (National Instruments Corporation, USA).

2.4.1 Belts

A light-weighed black velvet fabric with a white back side was used as the material for most of the belts (Velvet Fabric, 0.762 mm Thick, 1219.2 mm Wide, Plain Backed, McMaster-Carr, USA). The length of each track was 150 cm and the width 4.5 cm. To enrich the sensory experience of the animal on the belt, tactile cues were attached. As tactile cues, a combination of hot glue droplets, Eppendorf tube caps and shrinkable wire tubing pieces were used. As an additional cue and to increase the saliency of each patch, short pieces (3-4 cm) of fishing line were inserted upright into the hot glue droplets. The belt was divided to three, 50 cm zones with distinct patterns to provide a distinguishable experience of space for the mice. Care was taken to have repetitive patterns of cues, mixed with unique one in order to have a smooth transition from one patch to another [fig. 2.5.1 B]. As explained earlier, the borders were marked with black teaser film on the back side of the belt to provide hallmarks for a better position detection. Each

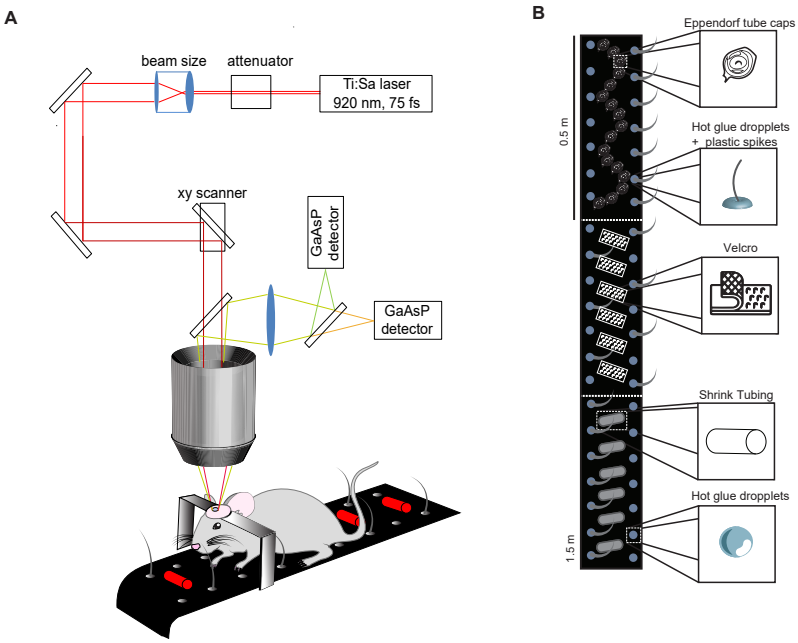

Figure 2.5.1: The two-photon light path and the cue enriched belt - A, a TiSi-laser generated 75 fs pulses, the laser beam was adjusted by an attenuator to fit into the back aperture of the objective. The emitted photons were then collected by two GaAsP detectors. **B,** we attached several different cues to make up three distinct tactile zones on the belt.

plain belt weighed 13 g and with the cues they weighed 32 gr.

2.5 Two-photon calcium imaging

We used a commercially available confocal microscope (A1 MP, Nikon, Japan) equipped with a 16X long-working-distance, water-immersion objective (CFI75 LWD 16X W, WD = 3mm, N.A: 0.8, XLPLN25XSVMP2, Nikon) controlled by NIS-Elements software (Nikon, Japan). The excitation wavelength for GCaMP6s was 920 nm, using a Ti:Sapphire pulse laser system (~75fs, Chameleon Vision-S, Coherent, Ireland). Emitted signals were detected by a gated GaAsP photomultipliers (H11706-40, Hamamatsu, Japan). The imaging was conducted using resonant scanners at the frequency of 15 frames per second (Hz) for duration of 20 minutes [see fig. 2.5.1 A, for a schematic of the two-photon light-path].

2.6 Behavioral paradigm

The behavioral paradigm used in this project was a modified version of context dependent fear conditioning as described in Lovett-Barron et al. 2014 and was adapted to our two-photon set up, head-fixed condition and available equipment in our lab. After a week of recovery following the virus injection and head-fixation implantation, the animals were habituated to the horizontal treadmill and the head-fixed running on the belt for a minimum of 10 min per day [for details check fig. 2.6.2].

One week after the surgery, *ad libitum* food was removed and a scheduled food diet according to the procedure explained in our animal-grant with AZ 84-02.04.2014.A254 and adopted from Wahlsten 2010 was administered. The food scheduling protocol was as follows:

Over the weekend (or the first two days of the protocol) the animals received a measured amount of food (e.g: 100 g). On the evening of the second day the remaining food was weighed in order to define the consumed amount by the animal over the two previous days. The value was divided by 2 and accordingly the equivalent amount of 1 g food pallets (Dustless Precision Pellets® Rodent, Grain-Based, Bio-Serve) was placed on the cage bedding. The animals weight was also measured and noted down. The weight and the consumed amount of food was supervised everyday and adjusted according to the general health and behavioral status of each animal until the animals reached to ~85% of their initial body weight. Throughout the food-scheduling period, a heat-pad was placed underneath the animal's cage to keep the temperature of the animal at 37°C.

During the behavioral performance on the belt, the animals received liquid food rewards at the end of each lap (diluted Butler Supplical Pet Multivitamin). As soon as they were accustomed to the belt and ran a minimum of 10 rounds per 10 min, the food scheduling was discontinued and hippocampal window implantation was carried out. After another week of recovery, the main behavioral experiments in combination with imaging started. The general outline of the paradigm was as depicted in the figure 2.6.1 extensively.

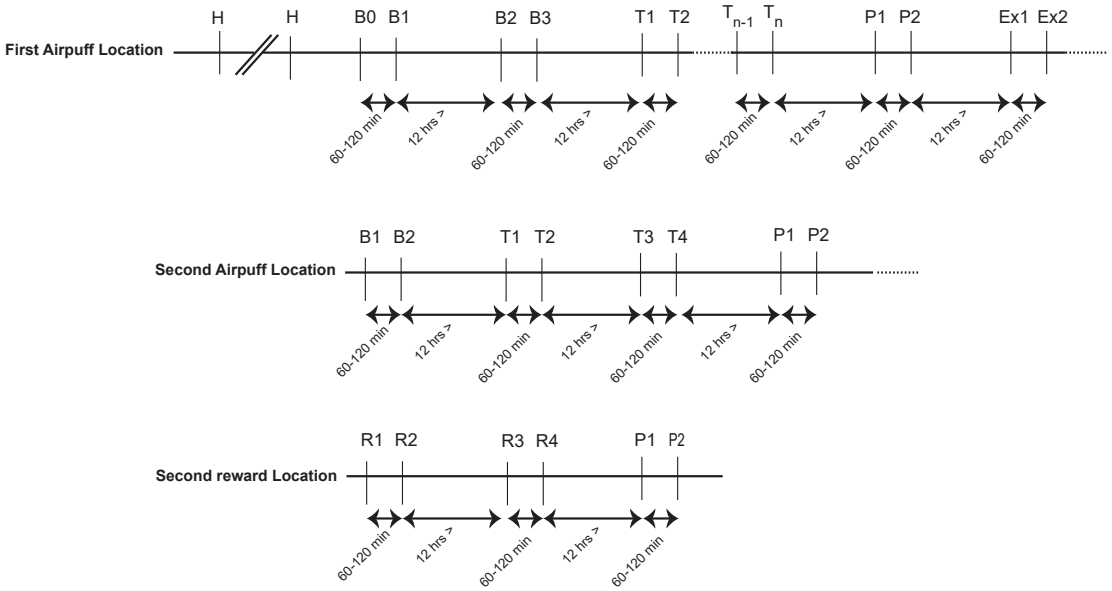

Figure 2.6.1: The general layout of the behavioral experiments - Generally animals were put twice per day on the belt, each time for a duration of 20 min, flanked by ~60-90 min (altogether 40 min per day). The upper line demarcates the first phase (the first airpuff location), during which the animals were initially habituated to the plain belt and the head-fixed running. Habituation (H) was then interrupted (double slash lines in the figure) for surgical procedures. After a recovery period, another period of habituation started and animals were food scheduled. As soon as achieving a satisfactory level of performance on the belt, baseline (B) period started. During the baseline sessions, animals ran on a cue-rich belt and received liquid rewards at the end of each lap. Training (T) sessions in the first phase included presentation of an airpuff stimulus, that was released as soon as the animal stepped into the second zone on the belt. Some animals required more than one training day (the dashed lines and Tn). Probe (P) session happened 24 hours after the last training session and there was no airpuff. In order for the animals to forget the memory of the first airpuff location, sessions of extinction (Ex) were carried out. The second phase (the second airpuff location), was identical to the first from B to P, except for the location of the presented stimulus. The animals were airpuffed on the third zone (at 100 cm). Finally, a sub-set of animals were tested in a reward-relocation experiments in which they were rewarded, instead of the end of each lap, at the borders between the second and the third zone for 2 days (R) and were tested 24 hours after (P) (data of the second airpuff location and reward relocation are not included in this thesis).

	Days	Session type	Condition	Duration	Description	Expectation
Food scheduling	Virus injection and head-fixation implantation followed by 7 days of recovery					
	1 day	Free exploration	Treadmill	2 × 5–10 min	Allowing the mice to freely explore the belt and sniff around	N/A
	2–5 days	Habituation (H)	Plain belt + reward	2 × 10 – 15 min	Familiarizing the mice to being head-fixed and running on the belt. Random reward delivery.	To get the mice comfortable with the head fixation and pushing the belt forward until they are stress-free.
	Hippocampal window implantation					
	Pause for recovery					

	Days	Session type	Condition	Duration	Description	Expectation
Food scheduling	1-5 days	Habituation (H)	Plain belt + reward	10-15 min	re-familiarizing the mice to being head-fixed and running on the belt and consuming the drops at 150 cm(end of a complete lap).	To get the mice run min. 10 rounds in 20 min and consume their drops
	2 days	Baseline (B) (40 min)	Cued belt + Reward	Tl1 (20 min) 60-120 min Tl2 (20 min)	the mice run on the cue-rich belt and receive a diluted liquid reward at the end of each completed lap.	To bring the mice to a smooth progression on the belt and regular reward consumption.
		Baseline (B) (40 min)	Cued belt + Reward	Tl1(20 min) 60-120 min Tl2(20 min)		
	2-5 days	Training (T) (40 min)	Cued belt + Reward + Air puff at 50 cm	Tl1(20 min) 60-120 min Tl2(20 min)	The mice run on the belt and receive air puff from the 3rd round in the first trial at a fixed location (50 cm). Second trial is the same except, the air puff starts from the first round on. They are also rewarded at the end of each lap as before.	To see a clear stop and slow-down reaction to the air puff.
		Training (T) (40 min)	Cued belt + Reward + Air puff at 50 cm	Tl1 (20 min) 60-120 min Tl2 (20 min)		
	1 day	Probe (P) (40 min)	Cued belt + Reward	Tl1(20 min) 60-120 min Tl2(20 min)	The mice receive no air puff. They are rewarded at the end of each lap.	It is expected to see a reaction to the previously experienced air puff location. E.g.: running speed reduction or complete stop
	1-2 days	Extinction(Ex) (40 min)	Cued belt + Reward	Tl1(20 min) 60-120 min Tl2(20 min)	The mice run on the cue-rich belt and receive a diluted liquid reward at the end of each completed lap.	This step has to be done until there is not sign of hesitation towards the air puff location and the animal runs as it ran during the baseline session.
	2 days	Baseline (B) 2-1 (40 min)	Cued belt + Reward	Tl1(20 min) 60-120 min Tl2(20 min)	The mice run on the cue-rich belt and receive a diluted liquid reward at the end of each completed lap.	To bring the animal to a stable performance without behavioral signs induced by air puff. This session can be excluded if the animal already has a smooth performance.
	2 days	Training (T) 2-1 (40 min)	Cued belt + Reward + Air puff at 100 cm	Tl1(20 min) 60-120 min Tl2(20 min)	The mice run on the same belt and receive air puff from the 3rd round onward in the first trial at a fixed location (100 cm). Second trial is the same except, the air puff starts from the first round on. They are also rewarded at the end of each lap as before.	It is expected to see, as the previous air puff location, a clear reaction to the AP, such as stopping or speed reduction.
		Training (T)2-2 (40 min)	Cued belt + Reward + Air puff at 100 cm	Tl1(20 min) 60-120 min Tl2(20 min)		
	1 day	Probe (P)2-1 (40 min)	Cued belt + Reward	Tl1(20 min) 60-120 min Tl2(20 min)	The mice receive no air puff. They are rewarded at the end of each lap.	As previous probe session, the ideal read- out is speed reduction to the new location of the AP.

Figure 2.6.2: The details of behavioral experiments.

Briefly, one day of *free exploration* consisted of two or three times placing the animal on the apparatus to sniff around and freely explore the environment and the belt, each time for a maximum of 10 minutes. This was then followed by days of *Habituation (H)*. Habituation sessions were the sessions in which the animals were head-fixed on the treadmill in order to get used to the situation and to eventually run smoothly on a plain belt and reliably consume the reward. Reward drops were given at the end of each lap. Such habituation days were repeated until the animals reached a steady performance and completed a minimum of 10 rounds in 20 min.

At this stage, the food-scheduling and training was interrupted by window implantation and a period of recovery after which, *Baseline (B)* sessions started. The two baseline sessions, consist of two 20 min of running on a new cue-enriched belt. The mice are rewarded upon successful completion of each round. The two baselines were followed by *Training (T)* sessions. During training sessions, animals received a puff of compressed air each time they passed the border of the first and the second zones on the belt (at 50 cm for the first round of the protocol). This condition was repeated for as many days as needed until the animals showed reliable slowdown or stopping behavior close to the airpuff location.

During the *Probe (P)* day, the airpuff was removed and the expectation was that the animals showed signs, indicating the memory maintenance of the previously experienced airpuff and stopped or slowed down at, or close to the airpuff location.

Extinction(E) sessions were one or at max. two days following the probe, for the animal to forget the learnt first airpuff location, and do not slow down or stop any further at 50 cm. In the extended form of the protocol, the extinction days are followed by new training days, with everything similar to the first training sessions, except for the location of the airpuff which this time was at 100 cm.

2.7 Immunohistochemistry

After the experiments, in order to verify a successful targeting of the injection site, animals were deeply anesthetized with ketamine (80 mg/kg body weight) and xylazine (15 mg/kg body weight). As soon as the confirmation of sufficient depth of anesthesia, the animals were transcardially perfused with PBS followed by 4% paraformaldehyde (PFA). The brains were then extracted and stored in 4% PFA for at least 24hrs. They were then rinsed with PFA with PBS (3x rinse) and sliced with a vibratome (Leica) to 70 µm coronal slices. For nuclear staining, brain slices were kept for 10 min in a 1:1000 DAPI solution at room temperature. Brain slices were mounted and the red, green and blue fluorescent channels were successively imaged using an Epi-fluorescent or spinning-disc microscope (Visitron VisiScope).

2.8 Data analysis

All the codes for the analysis of imaging data were written in MATLAB. Standard image-processing and calcium imaging toolbox and packages were customised for our purpose. The behavioral data was partly analysed in MATLAB and partly in Python (see section 2.8.4).

2.8.1 Calcium imaging movies

Prior to motion correction, the heavy periodic ripple noise inflicted by the GaAsP detectors was removed using a self-written fast Fourier transformation code (FFT) suited for this purpose. To remove the motion artifacts from the movies, for some, we used the Lucas-Kanade model introduced in Greenberg and Kerr 2009 and for the rest, the fast non-rigid motion correction (NoRMCorr) using the red imaging channel, with astrocytic labels, as the reference channel [109]. The fiber components, in the form of single fibers or networks were detected and their Ca^{2+} events were deconvolved using a constrained non-negative matrix factorization (NNMF) based algorithm [109]. The NNMF package written for dendritic data, treats the

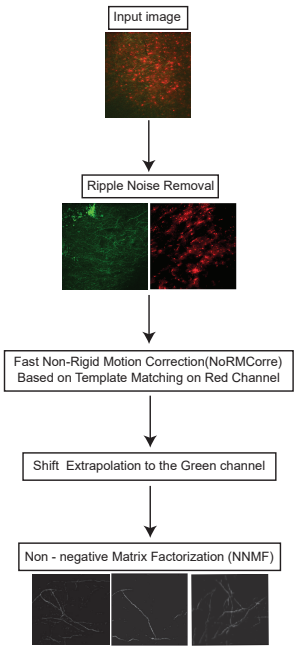

Figure 2.8.1: The image processing pipeline - As the first step, the dual channel movies were de-noised and then registered. The process of motion registration was a fast non-rigid motion correction, initially applied on the red channel with red fluorescent astrocytic markers, after which the calculated and corrected shifts were extrapolated to the green channel. As the last step, the components were extracted using a NNMF.

entire field of view (FOV) as one, and does not segment it into smaller grids, hence the components can be either single axons or several that had identical temporal profiles throughout the recordings. All the components were manually inspected, redundant components were rejected and those with a unique spatial profile and at least one Ca^{2+} were kept [fig. 2.8.1].

2.8.2 Spatial tuning

In order to assess the tuning of spatial information in CA3 axons, we devised spatial tuning vector analysis explained in Danielson et al. 2016. For the sake of this analysis, we used running epochs. We defined a running epoch as an episode of movement with a minimal duration of 2.5s above a threshold of 4cm/s in a forward direction. Only cells with minimum of 4 event onsets during running epochs were included in the analysis. The belt was divided into 150 evenly sized bins of 1 cm.

To take the circular structure of the treadmill into account, positions on the belt were translated into polar coordinates. An angle a_i was ascribed to every running related event and weighted based on the amount of time the animal spend at that position T_i.

The spatial tuning vector v_{space}, was then defined as the sum of all weighted event angles

$$v_{space} = \sum_{i}^{J} \left(\frac{a_i}{T_i} \right) \tag{2.1}$$

For normalization of this vector, it was divided by the total number of running related events, J, and with the average time per spatial bins

$$v_{space} = \frac{1}{j} \sum \left(\frac{T_i}{J} \right) \sum_{i}^{J} \left(\frac{a_i}{T_i} \right) \tag{2.2}$$

We addressed statistical significance by creating the null distribution for every spatially tuned cell. This was achieved by randomly shuffling the onset times and recalculating the spatial tuning vector 1000 times. The p value was calculated as the percentage of vector lengths arising from the

shuffled distribution that was larger than the actual vector length.

2.8.3 Axon tracking

In order to follow axons over days, we devised a cross-correlation approach. As a reference image, we used an average image of the FOV for each movie. The movies were recorded in two-channels, in which the red channel had astrocytic labels and the green channel included the axons. Initially, the red channel was used as the base of transformation for different imaging sessions. The spatial components in the green channel were then matched. A maximum shift of 10 pixels was allowed between the reference and the current component. Then the cross-correlation value of the components were calculated between the two days. The components with maximum cross-correlating r values were identified and the components with $r < 0.2$ were rejected. As the next step, the non-matching components were rejected. Figure 2.8.2 includes some examples of a few tracked components across behavioral sessions of interest.

2.8.4 Behavior

Contribution: the implementation of Hough transform on the speed per location data, and the calculations in this section were done by Dr. Fatemeh Kamali.

For isolating a learning behavior, we relied on changes in the running speed of the animal, the data of which was collected as explained in section 2.4 and the code was developed in Python with standard packages. The speed data was plotted as gray-scale images of speed per 1 cm space bins on the belt. This was done in order to find similar vertical lines due to the alignment of similar speed patterns in each round at the top of each other. Then a pipeline of image processing steps was implemented. First, image-thresholding was applied to create a binary segmented image with an 85^{th} percentile threshold. A spatial range around the reward location (0 cm to 10 cm, and 140 cm to 150 cm) was excluded from the analysis, due to the bias of the animals to have repeatedly stopped around the area.

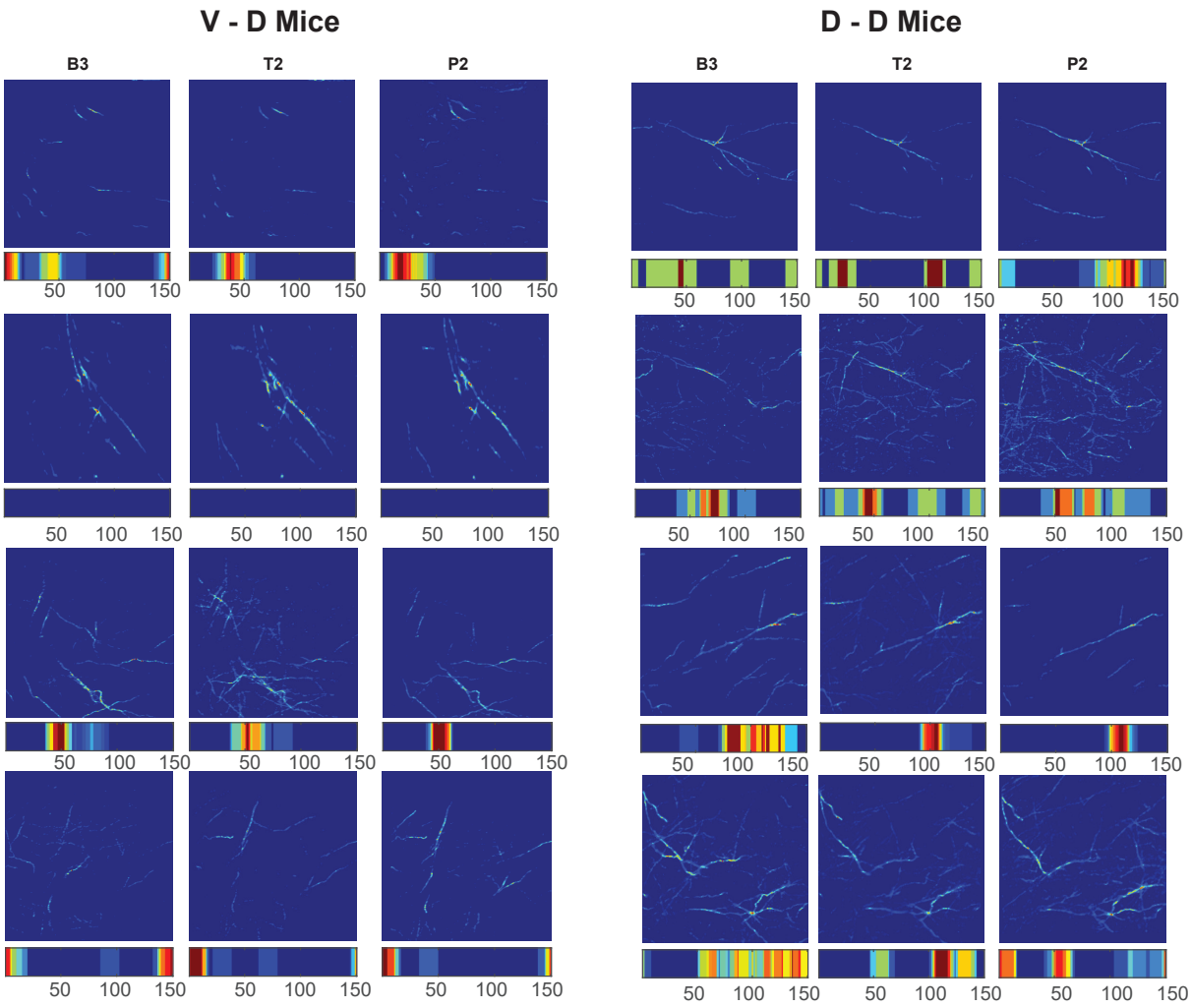

Figure 2.8.2: Successful axon tracking across multiple behavioral sessions - Using the cross-correlation algorithm we were able to find similar components over multiple sessions (the bigger squares in each row). Lower panels under each component, indicate place-related firing of that particular component along the belt. Panels in the left are examples of V-D animals and the right ones are examples of D-D.

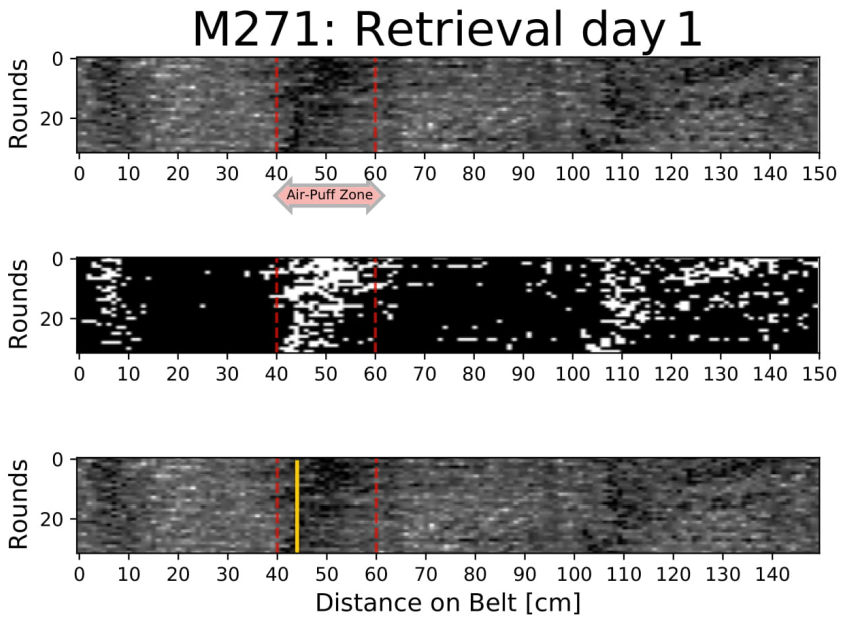

Figure 2.8.3: Mice speed on the belt - Top panel, the original image. Middle panel, the threshold image used for line detection. Bottom panel, shows the original image with the top voted line (in yellow) detected by the Hough transform algorithm. The airpuff zone is represented with vertical red dashed lines.

Next, a Hough-transform was used in search for vertical lines in the binarized image [56, 37]. Hough transform is a feature extraction algorithm that can find simple geometrical shapes, such as vertical lines or circles despite slight distortions. Consequently, a list of vertical line positions was obtained, each possessing a certain number of votes. The top voted line (or lines in case more than one line gets the highest number of votes) were then selected in baseline, training and, probe sessions. We then showed that the top voted lines in each animal during the baseline sessions were randomly distributed along the belt while on the training days, they were very close to the airpuff location and on the probe days the majority of the top-voted lines were restricted around the airpuff zone, indicating the mice memory of the airpuff location [fig. 2.8.3].

To investigate the null hypothesis that was, the presence of n out of m lines in the airpuff zone on the probe days being by chance, we used the null hypothesis significance testing. The aim was to reject the null hypothesis at

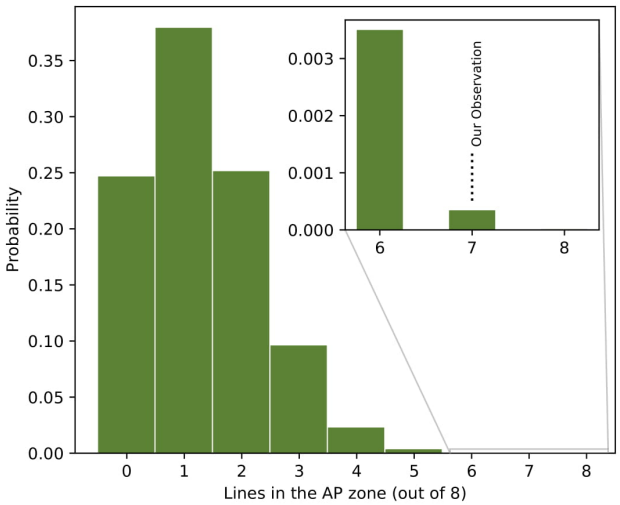

Figure 2.8.5: Probability distribution of count of lines (out of eight) in the airpuff zone, drawn from a uniform distribution of integers representing the belt without the reward zone. The small figure inside is a zoom-in on the tail of the distribution.

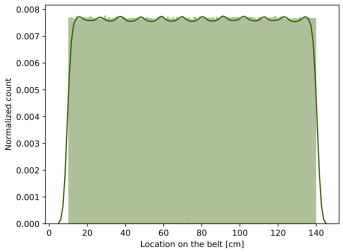

Figure 2.8.4: Random locations on the belt drawn from a uniform distribution of integers.

a cut-off level. Since no particular place on the belt should be favoured, we drew a sample of m line locations out of a uniform distribution of integers ranging from 10 to 140 [representing the belt excluding the reward zone, fig. 2.8.4]. The random selection process also allowed duplicate values to exist. We then counted the number of lines located in the airpuff zone in each sample. This procedure was repeated for one million trials. The probability of having n or higher number of lines in the airpuff zone, was defined as N_{n+}/N_m, where N_{n+} is the count of samples with n to m lines in the airpuff zone, and N_m was the total count of samples, in this case one million.

In all eight tested mice, the top voted line in the probe day 2 was in the airpuff zone. Only in 12 cases in one million trials of hypothesis testing, there was seven or higher number of lines in the airpuff zone. Since the obtained p-value of 0.000012 was smaller than the chosen cut-off level of 0.0001, the null hypothesis of seven out of eight lines being by chance in the airpuff zone at a 99.9988% confidence level, was rejected [fig. 2.8.5].

3

Results

3.1 Et-iCre CA3 specificity

In order to confirm the specificity of cre-recombination in CA3, we crossed the Et-iCre mouse-line with a *td-tomato* reporter line, which resulted into the expression of the red fluorescent marker in all the cells with cre-recombinase. We then performed a double immunostaining with anti-Dynorphin antibody to stain the mossy fibers and an anti-STEP antibody to label the CA2 pyramidal cells. The staining showed that the *td-tomato* expressing neurons had almost no overlap with cells labeled with STEP2, hence sparing the pyramidal cells of CA2 region and proving the exclusivity of Cre recombinase to CA3 cells [fig. 3.1.1].

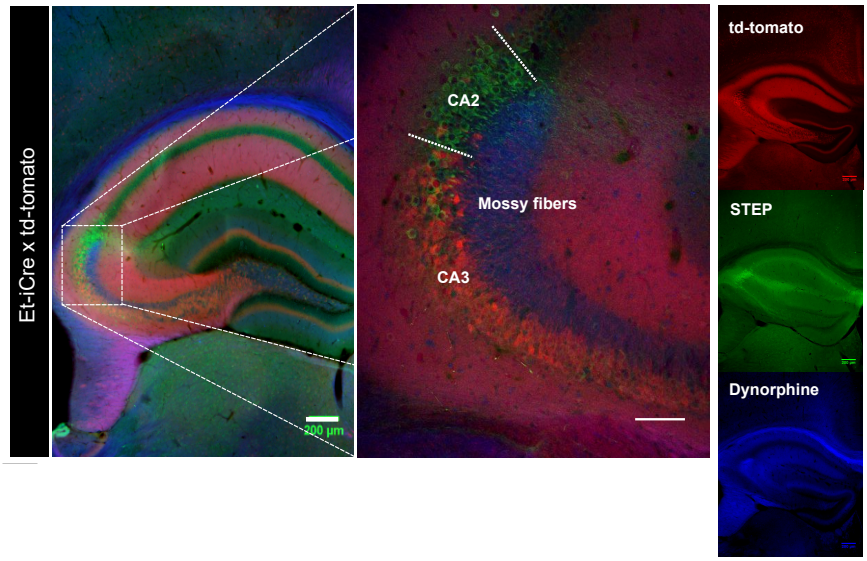

Figure 3.1.1: Double immunostaining of Et-iCre x *td-tomato* mouse line. Left panel: coronal section of the HP. Red: *td-tomato* expression in CA3 neurons. Blue: mossy fibers originating from DG GCs and terminating at the border of CA2 - CA1. Green: STEP2 labeled CA2 neurons. Middle panel: higher magnification of the same coronal slice. Right insets: separate channels showing *td-tomato*, STEP2, Dynorphine. Scale bars are 200 and 100 µm.

3.2 Activity of V-D and D-D CA3 axons during locomotion and immobility

In order to evaluate the information transfer between dorsal CA3 neurons, as well as ventral to dorsal CA3, we injected floxed-GCaMP6s in dorsal and ventral CA3 of the Et-iCre mice. Expressing floxed-GCaMP6s in the Et-iCre mouse-line resulted in robust expression of GCaMP6s in D-D [fig. 3.2.1 A] and V-D [fig. 3.2.1 B] axons. We then recorded Ca^{+2} activity of the GCaMP6s labeled single axons with a two-photon microscope [see section 2.5] while animals were head-fixed and ran on a linear track as explained in section 2.4. We first monitored the activity of axons during three baseline sessions ($B_{1\text{-}3}$) recorded in two consecutive days. For that, we imaged D-D axons [B1=167, B2=134, B3=119 axons, n=4 mice, fig. 3.2.1 A, C] and V-D axons [B1=136, B2=170, B3=181, n=4 mice, fig. 3.2.1 B, D]. Using NNMF we extracted single axonal components and their calcium activity [fig. 3.2.1 C, D]. We found that the activity of fibers were differently modulated during locomotion in V-D vs. D-D axonal systems. V-D axons showed a decreased discharge rate during locomotion [1.63 and 0.70 Hz for immobility and locomotion, respectively; Kolmogorov-Smirnov test,

p<0.05, fig. 3.2.1 E, yellow bars], while D-D had an increased average discharge rate [1.20 and 2.91 Hz for immobility and locomotion, respectively during B3, Kolmogorov-Smirnov test, p<0.05, fig. 3.2.1 E, green bars], this was consistent across all three baseline sessions. Upon closer evaluation, two population of neurons were observed in both V-D and D-D axons. First population had a low activity during periods of rest and increased their activity during locomotion. The second population showed an opposite behavior. Plotting locomotion and resting related activities confirmed the presence of axonal population being virtually silent in either of the two states [fig. 3.2.1 G, H]. We classified axons as locomotion-related or rest-related when the activities had a ten-fold difference. These two classes of axons were inversely distributed in V-D and D-D [69.6% vs. 10.1% in V-D and D-D axons, $\chi^2_{(2,N=138)}$=109.8, p<0.001], while dominant running-related activity was very rarely observed in V-D axons compared to D-D axons [2.8% vs. 24.36% in V-D and D-D axons, $\chi^2_{(2,N=34)}$=109.8, p<0.001].

3.3 Place representation in V-D and D-D axons

As mentioned in the earlier chapters, ventral and dorsal hippocampal neurons code the space differently. We identified CA3 axons that showed significant place-related firing. In both projections, place-coding axons tiled the entire length of the linear track [fig. 3.3.1 B, C]. Consistent with previous studies we found a significantly higher fraction of place-coding axons in the D-D compared to V-D [74.3 vs. 23.0% on average across the baseline sessions, χ^2 test for B3, $\chi^2_{(1,300)}$ =125.5, p=0.01 x 10^{-15}, fig. 3.3.1 D]. We then tested whether the precision of individual place-coding axons in these two axonal projections is different using place vector length measurement [the straight red lines in the polar plots fig. 3.3.1 A]. There was no significant difference with regard to place vector length between the D-D and V-D place-coding axons in none of the baseline sessions [fig. 3.3.1E, Kolmogorov–Smirnov test, n.s.]. Collectively, these results showed that V-D had a lower fraction of locomotion active neurons reflected also in their

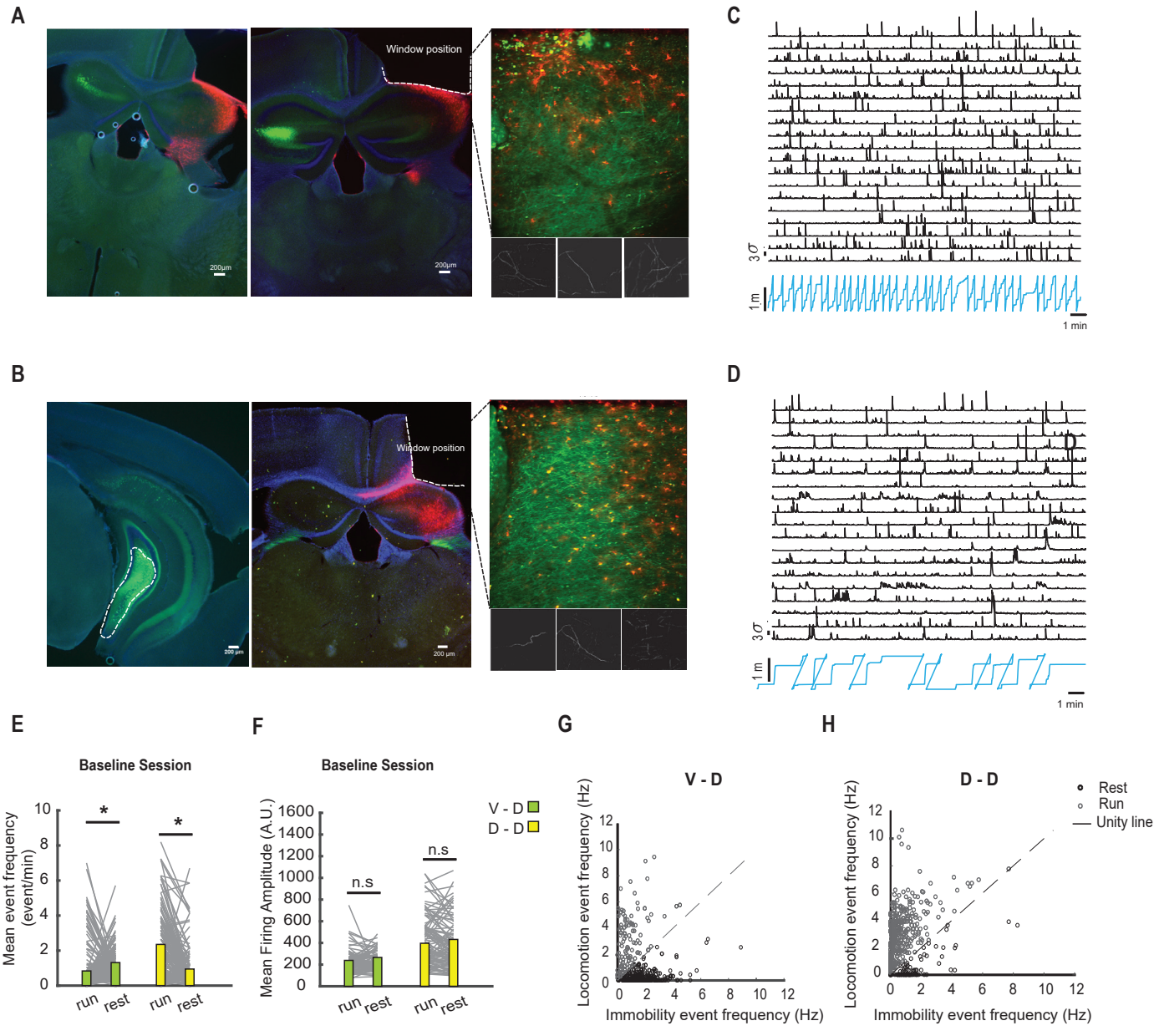

Figure 3.2.1: Activity of V-D and D-D CA3 axons during locomotion and immobility- **A,B,** post-hoc immunostaining of the injection site and expression profile of GCaMP6s and mCherry. **A,** coronal section of dorsal injection site shows expression of GCaMP6s in CA3 neurons on the left hemisphere (green) and mCherry expression in the astrocytes on the right hemisphere at the hippocampal window site (left panel). A more posterior coronal section of the same brain with the hippocampal window site (middle panel). The most right is a representative FOV of D-D axons imaged under the two-photon microscope. The small segments underneath are examples of extracted components with NNMF. **B,** similar to A for ventral injection site and V-D fibers. **C, D,** example of deconvoluted calcium traces for D-D (C) and V-D (D). The blue traces show the mouse position on the belt. **E, F,** mean firing rate (panel E) and amplitude (panel F) of V-D and D-D axons during locomotion (run) and immobility (rest). **G, H,** relation of activity during run against rest for each individual axon in the V-D (panel G) and D-D (panel H).

lower fraction of place-coding axons compared to D-D axons.

In order to check the efficiency of V-D and D-D axons in place prediction we used a generalized linear model (GLM). GLM was trained for the first 15 min of each trial on the belt and as the test phase, predicted the remaining 5 min of the trials [fig. 3.3.1 F]. Both axonal populations predicted space better than the shuffled data [mANOVA, $F_{(9.7)}$, p= 0.003 for location]. In line with the higher number of place-coding axons in the D-D projection, these axons predicted place significantly better than the V-D [mANOVA, $F_{(1)}$=10.1, p=0.0027].

3.4 Malleability of spatial codes in D-D and V-D axons during learning

After analysing the place-coding during the baseline sessions, we went forward and checked whether in the training sessions the airpuff's saliency is incorporated at the first airpuff location into the established place maps. The airpuff was given at the borders of the first and the second zones [see section 2.6 and fig. 3.4.1 A]. Mice usually quickly reacted to the airpuff and slowed down or completely stopped around the airpuff location as shown in figure 3.4.1 B. On average 3 days of training was needed to get a consistent behavior of slowing down near airpuff location [4.25 days on average for the V-D group and 2 days on average for D-D mice, T_1 is the very first session on the first day of training after baseline and T_n is the last session on the last day of training fig. 3.4.1 A and fig. 2.6.1]. By applying Hough transform on the speed per location heat-map data [see method section 2.8.4] we checked to see whether mice consistently stopped close to the airpuff location. Mice slowed down at random locations during the baseline sessions [fig. 3.4.1 B polar diagram and C, thresholded heat map example for B_3], while they consistently slowed down before the airpuff location [fig. 3.4.1 B and C, example for T_n]. Analysing the probe-day speed data also showed that after learning the animals still slowed down, close to the airpuff location, even in the absence of airpuff [fig. 3.4.1 B and C, example for P_1]. This showed that mice found airpuff aversive, reacted to it and consis-

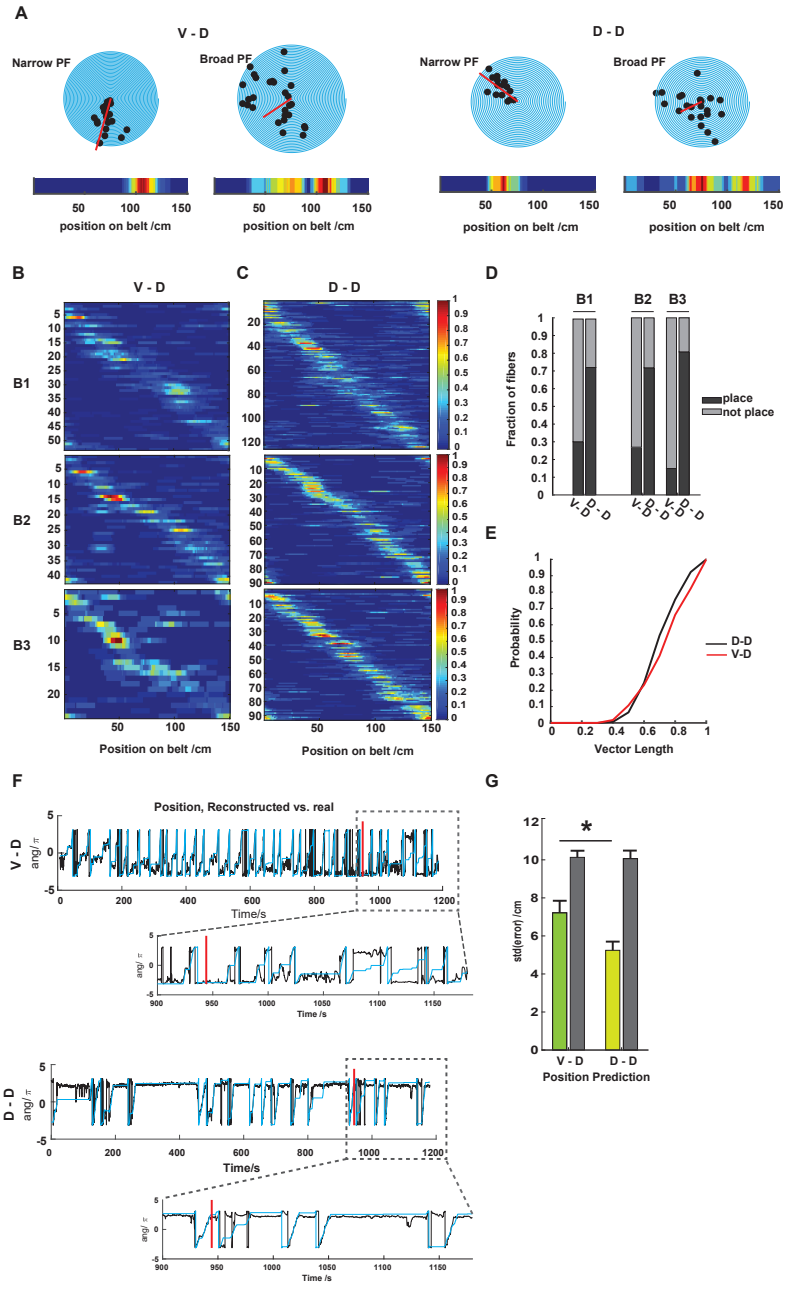

Figure 3.3.1: Place-coding in V-D and D-D axons- **A,** examples of place related activity depicted on polar plots where a complete lap on the belt is equivalent to 360°. Examples show a broad and a narrow place-coding axon for each V-D and D-D. Each black dot is a detected Ca^{+2} event; the straight red line is the summed vector of each individual event. The blue band underneath depicts the place-related firing as a heat-map. **B,C,** heat maps of place-coding axons in V-D (panel B) and D-D (panel C) axons in 3 baseline sessions, B_1,B_2,B_3. **D,** fraction of place-coding axons in V-D compared to D-D axonal population. **E,** place-coding precision assessed by vector length cumulative probability in V-D compared to D-D axons. **F,** place prediction by V-D and D-D axons assessed by a GLM model. The first 15 min of each trial was used as the training phase for the GLM (Red vertical line indicates the end of algorithm's training) and the last remaining 5 min was the test phase. **G,** prediction of position by GLM in V-D and D-D axons compared with the shuffled data (gray bars). Bars show averaged values of three baseline sessions (B_{1-3}). The asterisks show significance for ANOVA $p<0.05$.

tently acquired the memory of its location on the linear track [fig. 3.4.1 B]. We then assessed how the spatial code is altered during learning. For that we checked whether the overall fraction of place-coding axons is changed during learning. In the D-D axons, the fraction of place-coding axons remained high throughout learning [78% in B_3, 84% in T_1, 71% for T_n and 75% for the probe trial, fig. 3.4.1]. However, in the V-D axons this fraction seemed to increase [from 13% in B_3, 19% and 18.84% for T_1 and T_n, to 26% in the probe trial fig. 3.4.1 H]. There were no significant changes in the precision of place-coding in either of the projections [fig. 3.4.1 I, Kolmogorov-Smirnov test, n.s.].

In V-D axons we observed that the zone preceding the airpuff location became over represented during the training sessions [fig. 3.4.1 D for second training trial T_1 and T_n], this over-representation persisted also during the probe trial [P in fig. 3.4.1 D]. These changes were not as strong in the D-D axons [fig. 3.4.1 D, rightmost column, see representations for all sessions]. We quantified this phenomenon by translating each cell and its position on the linear track as a vector on a polar plot. The vectors on the polar plot point to the position on the linear track where the peak activity of that cell occurs and the length of the vector represents normalized peak of fluorescent activity [fig. 3.4.1 E]. Circular statistic analysis on the polar plots showed that the distribution of these vectors was nonuniform in the last training and probe session in the V-D but did not prove a significance in the D-D [Hermans–Rasson test, B_3: $p = 0.74$, T_1:$p = 0.06$, T_n: $p = 0.05$, P: $p = 0.01$ for V-D; and B_3: $p = 0.77$, T_1: $p = 0.62$, T_n: $p = 0.06$, P: $p = 0.55$ for D-D]. Moreover, the summed vector reliably pointed into the direction of the pre-airpuff zone in all training trials and P in the V-D [bold lines in fig. 3.4.1 E, quantification of place cell proportions for the three linear track zones in fig. 3.4.1 F, G]. These data suggests, despite the lower number of place-coding axons, V-D axons start incorporating the location of the aversive stimulus during training.

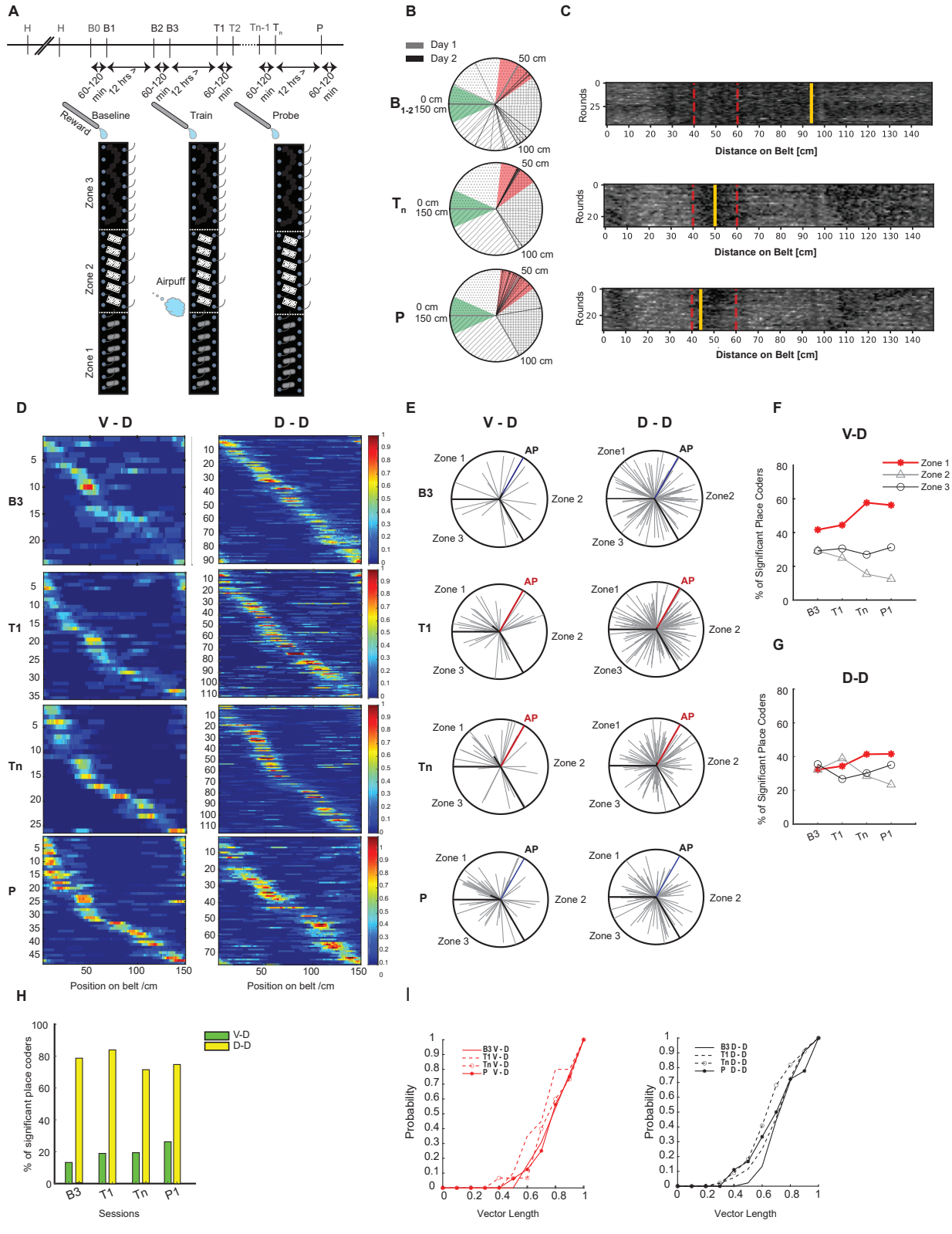
A
H
H
B0 B1
B2 B3
T1 T2
Tn-1 Tn
P
60-120 min
12 hrs
Baseline
Train
Probe
Reward
Zone 3
Zone 2
Zone 1
Airpuff
B
Day 1
Day 2
B1-2
Tn
P
0 cm
150 cm
50 cm
100 cm
C
Rounds
Distance on Belt [cm]
D
V - D
D - D
B3
T1
Tn
P
Position on belt /cm
E
V - D
D - D
AP
Zone 1
Zone 2
Zone 3
F
V-D
% of Significant Place Coders
B3
T1
Tn
P1
G
D-D
H
% of significant place coders
V-D
D-D
Sessions
I
Probability
Vector Length
B3 V-D
T1 V-D
Tn V-D
P V-D
B3 D-D
T1 D-D
Tn D-D
P D-D

3.5 Stability of place maps across sessions

Using axon tracking as explained in section 2.8.3, we examined how do changes in place-coding happen at the resolution of single axons. Particularly we wanted to see how the over-representation of the zone preceding the airpuff location forms during training. For this purpose we systematically analysed changes in individual axons across different pairs of sessions.

We compared transitions that had a time interval of more than 19 hrs between them. Specifically, the baseline trials (B_1-B_2) compared to transition from the last baseline to the first training trial (B_3-T_1), compared to the fist training session and the last (T_1-T_n) and the training trial and the first trial for the retrieval of memory (T_n-P_1)[fig. 3.5.1 A, B].

We first addressed the issue of place-coding stability. To this end, we checked whether the significant place-coding axons in the first of each combination of two consecutive sessions remained significant coders in the second as well. This was done disregard of zones and on the overall length of the belt. The number of axons that remained significant place-coding axons in the second session was higher in D-D compared to V-D in the B_1-B_2 [D-D: 41% and V-D: 34% in B_1-B_2].

Figure 3.4.1 ***(preceding page)*****: Malleability of spatial codes in D-D and V-D axons during learning**- **A,** schematic of behavioral protocol; the animals learn the location of an aversive stimulus while running on a cue-rich belt. **B, C,** isolated learning effect shown using Hough transform. The top-voted lines in baseline, training and probe sessions shown on the polar plots proved learning and consistent stopping around the airpuff location (red-demarcated area +/-10 cm) during training (T) and probe (P) but not the baseline (B). Examples of binarized images of speed per location bins. The yellow lines indicate the top-voted line by Hough transform, showing the consistent pattern of slowing at a particular area on the belt. Airpuff zone (+/- 10 cm from airpuff location) shown with dashed red lines. **D,** the place maps of the last baseline session (B_3), first training session (T_1) and the last training (T_n). **E,** polar plots with vector representations of the place preference of all place-coding axons, with the vector direction representing the position of peak activity, and the length of the vector representing peak normalized $\Delta F/F$. **F, G,** average fraction of significant place-coding axons on three zones, zone 1 being the zone preceding the airpuff location (0-50 cm, red) and the two other zones (50-100, gray) and (100-150, black), during baseline, training and probe trials in V-D and D-D axonal population. **H,** fraction of place-coding axons in baseline, training and probe trials. **I,** place-coding precision assessed by vector length in baseline, training and probe trials of V-D and D-D axons.

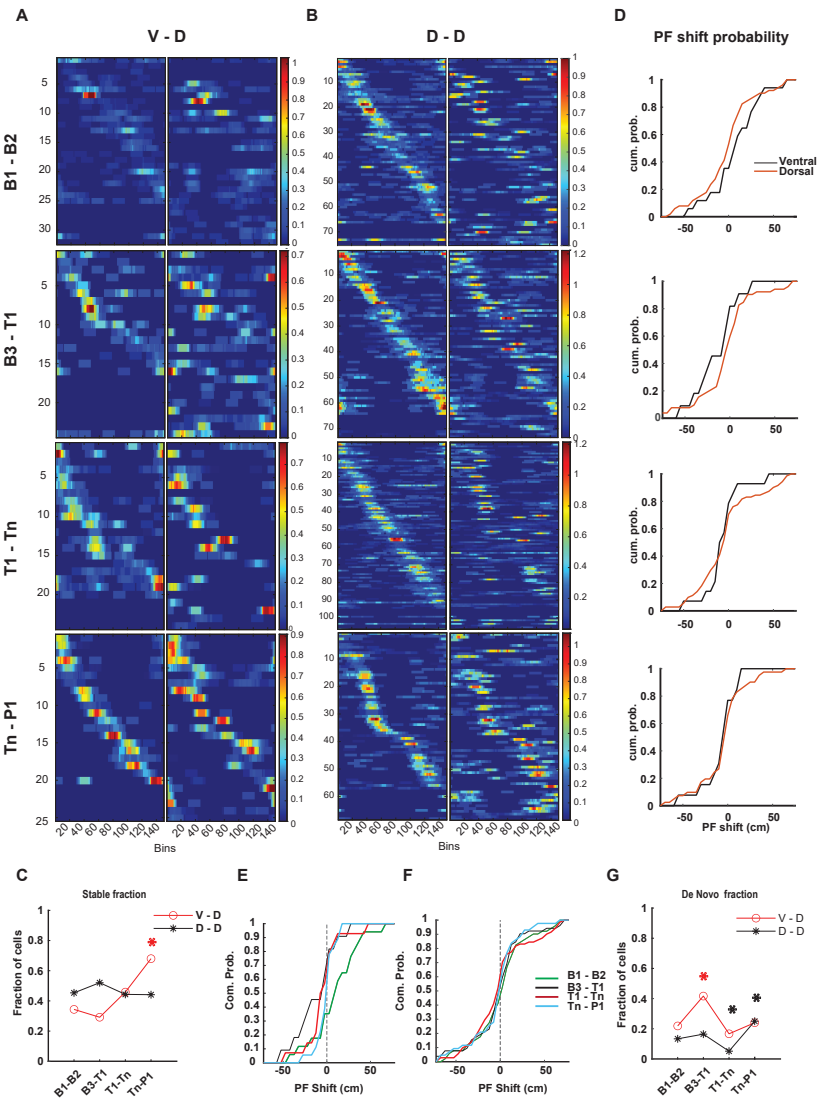

Figure 3.5.1: Stability of place maps across sessions - **A, B,** place maps of tracked axons across each session pair with overnight time interval (>19 hrs) for V-D (A) and D-D (B) axonal population for 4 transitions of B_{1-2}, B_3-T_1, T_1-T_n and T_n-P_1. **C,** the stable fraction of axons across session pairs mentioned in A and B. Notice the fraction of stable cells increases in the V-D population as the learning starts and increases from the last training session (T_n) to the probe session (P_1). Asterisks indicate significance of adjusted residuals. **D,** the place cells' center shift probability across the transitions. The shifts opposite to the running direction are depicted as negative values with regard to the original place center position in the first of each two session pairs and positive when they are in the direction of run. The plots show that the shifts are insignificant, hence persisting cells between session pairs do not remap significantly. **E, F,** place field shift comparison for session pairs mentioned in A and B for V-D (E) and D-D (F). **G,** the fraction of newly emerging cells in transition pairs. The biggest emergence happens in the V-D from the last baseline session to the first training session (B_3-T_1) and for the D-D in the memory maintenance phase (T_n-P_1)

During learning there was a significant increase in the number of stable place-coding axons in the V-D but not in the D-D [D-D: 44% and V-D: 45% in T_1-T_n]. This level stayed high inasmuch as V-D fraction of stable place-coding axons exceeded that of the D-D [D-D: 59% and V-D: 68% in T_n-P_1 fig. 3.5.1 C].

We then wanted to evaluate the shift in place centers of these stable place-coding axons across sessions. For this purpose, we quantified the shift of place centers between each two combinations of sessions. We found that shift of place centers between the B_1-B_2 was not significant in V-D compared to D-D [unpaired *ttest*, p = 0.25, fig. 3.5.1 D, top panel, p value n.s for all the other comparisons]. Similarly, comparing the within groups shifts in T_n-P_1 and T_1-T_n to the baseline B_1-B_2 transition, proved to be nonsignificant [for V-D ANOVA, $F_{(3,56)}$=2.65, p=0.057, for D-D ANOVA $F_{(3,213)}$=0.2, p=0.89, fig. 3.5.1 E, F]. This shows that as learning proceeds the stability of place maps increases but the center of place-coding axons do not shift significantly.

The changes in the place maps could also arise from newly emerging place-coding axons. To address this possibility we evaluated another category of fibers that emerged in the second session of each consecutive combinations. We call this category the '*de novo*' axons, which are the tracked components that did not qualify as significant place-coding axons in the previous session but are coding for place in the current session for the aforementioned transitions.

The fraction of *de novo* place-coding axons was significantly higher than expected at the onset of learning in V-D axons [B_3-T_1, Omnibus test over all sessions and categories $\chi^2_{(11,91)}$=12.7, p=0.048, fig. 3.5.1 G]. In contrast, D-D axons displayed a significant increase in *de novo* axons during memory maintenance [T_n-P_1, Omnibus test over all sessions and categories $\chi^2_{(11,241)}$=15.2, p=0.019, fig. 3.5.1 G].

3.5.1 Spatial preference of stable and *de novo* axons on the belt

We then examined whether the stable and *de novo* axons showed a spatial preference on the belt during different stages of behavior. For this purpose we presented all stable axons with a place vector on the polar plot representing the belt and the three zones (as it was done in the fig. 3.4.1 E). Then we calculated the summed vector. We noticed that, at the later stages of learning there was a significant number of stable axons in the pre-airpuff zone in the V-D axonal population [zone 1, fig. 3.5.2 A left panel, Hermans–Rasson test p=0.015, Rayleigh test p=0.04] but not in the D-D. In the D-D axonal population in all the transitions axons seemed not to show any significant zone preference and although not evenly, but occupied all the three zones [fig. 3.5.2 A right panel, Hermans–Rasson test, p=0.69, Rayleigh test p=0.56].

As for *de novo* fraction of axons, both axonal populations showed a significant place preference at the transition from learning to retrieval [T_n-P_1, fig. 3.5.2 B]. In V-D axons *de novo* axons occurred preferentially in a cluster, at the border of the pre-airpuff zone in V-D axons [fig. 3.5.2 B, left plot]. In addition, D-D *de novo* axons exhibited a spatial preference, almost completely sparing the post-airpuff zone of the linear track [zone 2, Hermans–Rasson test, V-D, p=0.01 and D-D, p=0.037, Rayleigh test, V-D, p=0.009 and D-D, p=0.005].

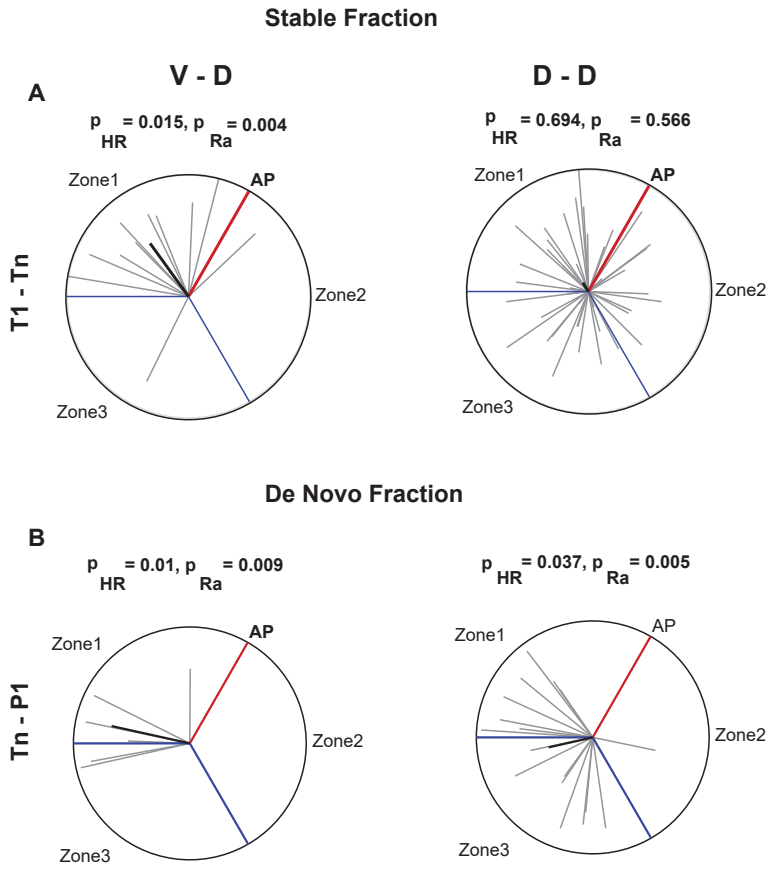

Figure 3.5.2: Place preference of stable and *de novo* axons- **A,** the stable category of axons seem to preferentially code the pre-airpuff zone in the V-D during the learning period. **B,** during the retrieval, the newly place-coding axons or the *de novo* show an increase with spatial preference to a zone in both V-D and D-D axons. Left plot: in the V-D this increase signifies the importance of the zone preceding the AP. Right plot: the *de novo* axons in the D-D seems to be more distributed in the third zone on the belt.

4

Discussion

In this dissertation we measured and described the different coding properties of two intrahippocampal long-range axonal projections: 1) the CA3 longitudinal projection (V-D), spanning the septotemporal axis and 2) the CA3 commissural fiber system (D-D), crossing the brain hemispheres. In order to measure their respective properties *in-vivo*, we devised an approach that allows us to image the activity of these axons separately using two-photon Ca^{2+} imaging and a behavioral paradigm in which the mice had to experience space-linked aversive stimuli in a single environment. The purpose of this paradigm was for the animals to form a memory of the aversive stimulus and later on retrieve the acquired memory, while we simultaneously imaged the activity of aforementioned projection axons.

With this approach, we could measure differences between V-D and D-D projections in terms of their general place-coding properties and address how the two axonal systems incorporate aversive stimuli into their existing

place maps. Furthermore, day to day precise adjustment of FOVs using dual-color imaging as well as a novel correlation analysis allowed us to successfully track individual axons across behavioral sessions. Tracking axons made it possible to describe the stable place-coding axons as well as those axons that acquired new place-coding properties (*de novo*). Considering these two identified categories of axons, we could uncover differences in stability or adaptability of V-D and D-D axonal population. We could also prove that there is a spatial preference for stability and recruitment of *de novo* axons on the linear track.

In this chapter, I will briefly discuss the techniques we used to conduct our experiments, their advantages and limitations as well as methodological challenges we faced along the way. I will then discuss the experimental results and their relationship with the existing knowledge about CA3 and the HC.

4.1 Methods discussion

4.1.1 Calcium indicator

Fluorescent calcium signals are extensively used for monitoring activity of populations of neurons. Optical imaging allows non-invasive registration of many axonal projections, relatively free of stimulation artifacts. Compared to chemical Ca^{2+} indicators, genetically encoded calcium indicators (GECIs) are efficiently delivered into a specific cell type or subcellular compartment and chronic imaging of Ca^{2+} indicators is less invasive [141]. For our experiments, we used GCaMP6s which has a time-to-peak of 179 ms and decay time of 550 ms [26]. GCaMP6s is capable of resolving supra-threshold events. Small fluctuations in a signal correlating to sub-threshold Ca^{2+} events are most likely a reflection of contamination by surrounding neuropil activity.

Although specific axon-targeted GCaMP6s have been developed [18], we achieved sufficient expression and satisfactory levels of signal-to-noise ratio with normal somatic GCaMP6s in our axons of interest. GCaMP6s

has proven to provide the highest yield of responsive cells compared to GCaMP6f and GCaMP6m [26]. We significantly improved the optical properties of our insert and hippocampal window and hence acquired satisfactory recordings of axons in both V-D and D-D injections. The axons in our study, showed bright and clearly labeled structures 2-4 weeks after the injection [for further details please check: section. 2.2 and fig. 3.2.1].

For smaller number of action potentials GCaMP6s is a very sensitive indicator and produces more than 10-fold larger signals compared to GCaMP3 [26]. The decay-time of GCaMP6s is slower than the other GCaMP6 constructs, however, when focusing on the rise-time, GCaMP6s has the sensitivity of resolving almost 100% of single spikes in bursts of action potentials. In our analysis we mainly focused on the transient onsets, therefore, GCaMP6s proved to be the most sensitive sensor.

Nonetheless, because the duration of somatic Ca^{2+} response is about 1.0 s, the response frequency is too low to reflect most network oscillations. In axons, the Ca^{2+} response can be even shorter and GCaMP6s cannot keep up with high frequency network oscillations, specially because of its higher affinity to Ca^{2+} compared to other GCaMPs such as GCaMP5G (3-fold higher affinity in this case)[26].

We could image the GCaMP6s expressing axons more than two months after the viral injections. Only after this time period, could we see few fibers with static fluorescence. It was also mentioned in Chen et al. 2013 that after several months of imaging (1-2 month in mouse primary visual cortex), high GCaMP6s expressing neurons gained nuclear expression [1]. Bleaching was also negligible, since the baseline fluorescence did not change over more than 60 sessions of imaging (20 hours).

With regard to the injection coordinates, there was some variability in the extent of virus expression along the longitudinal axis across different animals [fig. 4.1.1]. This could be due to slight deviations from the injection coordinates or differences in the size of the animals. Despite this, physiological and neural correlates provided evidence that we indeed targeted different populations of neurons; the number of fibers qualifying as place-coding axons (not the total number of detected fibers) was sig-

[1] Expression of GCaMPs is normally cytoplasmic. However, it has been reported that long term expression of GECIs in cells, breaches the nucleus integrity and neurons gain bright nuclear expression of GECIs. Neurons with filled nuclei show attenuated GCaMP fluorescence responses and reduced Ca^{2+} changes induced by neural activity. Also, spontaneous Ca^{2+} transients of nuclear-filled neurons show longer decay times which is another sign of abnormal physiology [141].

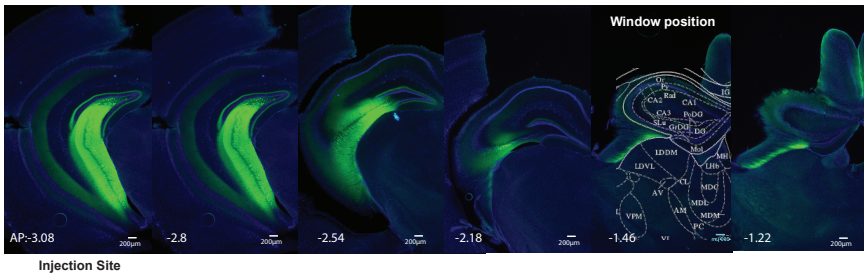

Figure 4.1.1: Ventral injection of GCaMP6s and the spread along the septotemporal axis- Typically 300nL of pAAV.Syn.Flex.GCaMP6s. WPRE.SV40 (AAV1) was injected in the ventral (ipsilateral to the window position. AAV1 spread was about ~1mm, covering a range of ventral to intermediate CA3.

nificantly lower in the V-D population compared to D-D population [fig. 3.3.1 D]. This fits the existing evidence regarding the higher levels of place-coding in dorsal HC compared to ventral HC, even though in the ventral injections, we might have labeled intermediate parts of the HC.

4.1.2 Behavioral paradigm

As mentioned earlier in our experimental design, we aimed at establishing a paradigm that harbors both components of space and aversion in order to engage both dorsal (spatial) and ventral (emotional) portions of the HC. In our experiments, we took the general design of head-fixed fear-conditioning paradigm first introduced by Lovett-Barron et al. 2014. Inspired by Lee et al. 2004 work and considering the fact that mice have the ability to scan objects by their finger tips and their whiskers and form sequences of tactile experiences, we built a zoned belt, covered with various tactile cues. Experiencing a sequence of sensory events–here the sequence of tactile zones on the belt–is expected to involve the HC [57, 23]. We hypothesized that unique proximal tactile cue recognition results in engaging the dorsal hippocampal place-coding, thereby involving the dorsal HC. We further hypothesized that presentation of a mildly aversive airpuff at one of the zones, would engage the ventral part of the HC.

The belt used in our experiments acts as a repeating sequence of tactile experiences in a short time scale. Studies like Lee et al. 2004 and Leutgeb et al. 2006 hinted that subtle changes in the actual sensory cues (change of color of the walls of an exploration arena) or the order of presentation of the cues (counter-clockwise rotation of the circular arena) is quickly no-

ticed by the animal, and is incorporated in the neural representations of CA1 and specially CA3 regions. There are number of technical points to be considered about our fear conditioning paradigm, explained in the following paragraphs.

In designing the cues, care was taken to make them haptically salient while allowing the animal to run on the belt without hindrance (e.g. by not making the belt too heavy or by obstructing the running path). The placement of cues on the belt created unique segments that changed every 50 cm. The borders of neighboring textures merged into one another smoothly to prevent sharp transition points that could act as cues for the airpuff.

The airpuff intensity and location are two critical points and were finely adjusted to be optimally aversive to the mice. The airpuff tube has to be positioned in a distance to deliver an appropriate intensity of the airpuff to an area of the mice's face. If too aggressive and close to their eye, animals tend to keep one eye closed and sometimes stop running completely and if too far, they tend to be indifferent to the stimulus. Our tube was laterally positioned at about 1 cm from the snout and released 9 psi of compressed air for 20 ms. The solenoid valve gating the airpuff was covered in foam and was placed furthest possible from the mice and the treadmill to prevent the animal linking the gating sound to the upcoming airpuff.

With regard to the behavior at the outset of the experiments, we noticed large performance variability in the distance that mice covered on the linear track. To minimize this variability, we decided to, 1) keep the animals motivated and, 2) increase the number of trials performed in a single experimental day. For motivation, we rewarded the animals at the end of each lap. Although reward did not eliminate performance variability, it motivated the animals to cover higher number of rounds per session (minimum of 10 round per 20 min). After the animals went through two baseline test days [and were assumed to have] formed a stable place representation of the belt, training on the airpuff location started. This period was another source of variability among animals. Not every animal showed signs of learning during the first training day, hence, days of training had to

be repeated for some of them. Since in the head-fixed fear learning the animals have no choice to avoid the airpuff and have to pass its location to complete the lap anyway, mice developed different strategies. For instance some stopped multiple times prior to the airpuff location, some ran faster at the airpuff location, or in general they completed lower number of laps. In hindsight, perhaps a better approach would have been giving the animals an option to avoid the airpuff. For example, in case of stopping before the location, no airpuff would be given. This could potentially lead to a better performance based read-out of the learnt location.

To quantify behavioral read-outs, initially, we relied on the speed changes of the animal. This was due to the limited possibility of food or water deprivation. Speed turned out to be a very complicated read-out because most of the mice stopped at multiple points on the belt and our speed sensors picked up small fluctuations. Therefore, this made the read-out noisy and difficult to interpret. To have a more uniform pattern of stops, we repeated the training sessions until the stops before the airpuff location were robust. With this approach, we minimized the performance variability to a reasonable extent.

Monitoring the eyes and pupil, counting licks or as mentioned earlier, short stops to avoid the puff could serve as additional learning measures in future experiments. Pupil diameter has been mentioned as a proxy for motor activity, cognitive effort or arousal states. In mice specially, changes in the pupil size are particularly thought to be linked with episodes of attention and arousal [114, 77]. As for the lick-counting, conditioned lick-suppression has been used as a standard measure of fear-learning [17, 89]. Finally, with availability of tools such as DeepLabCut, it is possible to monitor animal's facial expressions during task performance. Monitoring saccades, whisker movements, or even subtle muscle twitches could depict a more sophisticated picture of the behavioral read-out [90].

Another critical factor in the behavioral task is the positioning of the lick-port. If the lick-port is placed too close to the snout, the animal licks compulsively and if it is placed too far, it misses the reward and loses motivation. We adjusted this distance for each individual animal depending on

its size but in general, it was between 0.5 mm and 1 mm from the lower lip.

With regard to food scheduling, although a general rule of 85% of the original body weight is given in the literature, there is a balance between weakness due to starvation and not being hungry enough to run for the rewards. Thus, every individual animal has an ideal body weight in which they are hungry and motivated but also not weak for repeatedly and consistently pushing the belt. To reach this optimal performance-weight, one has to train and adjust each animal's weight prior to the actual experiments.

As for the sex of the animals, we used both male and female adult mice (6-12 weeks). In order to get rid of the urine odor of male mice and avoid stress, after each experiment the set-up was cleaned with Ethanol 70% and isopropanol and the belts were removed. After each trial, time was given for the odor to dissipate. To avoid olfactory confounds due to a prior tested animal, the order of mice put on the belt for behavioral sessions was constant. Most importantly each animal (or cage mates) had individual belts assigned to them.

4.1.3 Motion correction and component extraction

In order to extract the components of recorded movies, there is a set of prepossessing steps required. Denoising and registering are two important preparatory steps.

We initially faced the challenge of a strong ripple noise (amplitude of a few μV to 3 mV and 300 kHz of frequency band) that covered the entire FOV and masked the dimmer interesting signal of the active fibers. We found that the noise pattern changed depending on the modes of scanning (e.g., uni-or bidirectional, with or without averaging, etc.) and that it was due to the high-voltage circuit oscillations inside the GaAsP photomultipliers (PMTs). Upon several hardware optimization steps, (e.g., raising the control voltage to increase the PMT gain) although reduced, the noise was not eliminated and having noise free recordings proved to be impossible. We therefore, had to remove the noise post-hoc by a self-adjusted FFT code.

In the image processing pipeline, as the next step, one has to stabilize the denoised movies. In the axonal imaging, since axons have no baseline fluorescent at the times that they are not active, detecting the same structures in one frame to another is difficult. Hence, even most powerful motion-correction algorithms fail to perfectly register the movies. For this problem, a repeating pattern of structures that fluoresces all the time, in the second imaging channel, could solve the issue. To this end, I tried several viral constructs tagged with red-fluorescent proteins to serve as a fiducial marker (e.g: AAV-GFAP-TurboPF650, pAAV-hGFAP.floxed-mCherry, pAAV-GFAP-mCherry). pAAV-GFAP-mCherry yielded uniform and regular labeling of the astrocytes and provided a base for motion-correction.

We used a constrained NNMF - based (CNMF) algorithm that was made available by Pnevmatikakis et al. 2016, to extract the spatial footprint and the temporal activity of axons. This modular approach in principle simultaneously handles factorization, deconvolution and denoising of Ca^{2+} signals in the recorded movies.

A key advantage of CNMF for axonal imaging is the ability of the method in extracting sparse, separated spatio-temporal components, despite the high spatial overlap of the axons [110].

As mentioned earlier in chapter 1, the large variability between boutons of the same axon could make the interpretation of Ca^{2+} signals hard and render them prone to error. Also, the influence of neuromodulators and postsynaptic cell types would make the aggregate measures ambiguous and biased toward the terminals with larger Ca^{2+} transients [1].

CNMF method detects axonal units and extracts their fluorescence changes across the entire length of the detected neurite in the FOV (as opposed to individual boutons) [109]. This approach minimizes some of the mentioned problems regarding interpretation of the Ca^{2+} signals at single boutons or aggregate measures; problems such as the bias of postsynaptic cell type, or the bias towards sub-population of boutons with larger amplitudes.

This however, equivocally serves as a negative point for axonal data, be-

cause network activities and synchronously active axons are presumed as a single component and untangling individual axons contributing in a network event, specially in large FOVs is not simple.

There are other qualitative differences in the application of this method for somatic versus axonic data. Parameters such as unit size (approx. size of a soma of a neuron), the τ- standard deviation of gaussian kernel for initialization - and number of expected components are not defined for axons as for soma. This is due to the mentioned fact that axonal branches can stretch everywhere in the FOV and have different sizes, their diameter is thin and almost negligible. In other terms, each spatial component although sparse, is no longer spatially localized. This issue could also influence the temporal domain and deconvolution of the Ca^{2+} signal. The dynamics of Ca^{2+} transients differ in axons due to differential Ca^{2+} source compared to somatic Ca^{2+}.

Additionally, the number of estimated components is defined by the user for the algorithm. This can artificially push CNMF to break spatially larger components into smaller ones. Basically, in the case of axonal movies, it can be too large and too small and defining the right value is challenging. In order to define the best component-number, we used an iterative approach in which spatial cross-correlation of components were checked, the ones with high spatial overlap were merged and the remaining ones were fed back into the CNMF algorithm. This approach yielded 80-100 components.

The other measure we took was to carefully and manually inspect all the components after extraction using a GUI. We rejected the ones that looked spatially either redundant or unusual and accepted the ones that had a proper spatio-temporal profile. We also merged again the components that looked like sub-components of one another. With these careful inspection steps we made sure we get the most spatio-temporally accurate final set of components.

4.1.4 Fiber tracking

Computationally, it is not a trivial task to identify and trace axons across multiple behavioral sessions. Despite careful day to day adjustments, small z-shifts are inevitable and due to the thin structure of axons, even small shifts in the FOV could affect the results. To follow fibers, we used a cross correlation-based method established in the lab [for details see 2.8.3]. The algorithm used astrocytic channel (red) as a reference, found similar structures and aligned any number of given sessions accordingly. Similar spatial structures were then identified in the axonal (green) channel and the ones with high correlation coefficient ($r \geq 0.2$) were accepted. We performed a manual inspection after fiber tracking to make sure that indeed similar structures were identified. One issue to be taken cautiously is the interpretations of the emerging and disappearing fibers which might be due to the algorithm having failed to detect similar axons in one of the sessions. Nonetheless, using this method we could track a reasonable number of axons successfully for the first time (up to 100 axons in both axonal populations).

4.2 Discussion of Results

4.2.1 Spatial coding in V-D and D-D fibers

In the **V-D axonal population**, during the baseline, a small number of place-coding axons represented the belt, with no zone discrimination. This low number provided a less accurate place map compared to the D-D population [fig. 3.3.1 B, D and fig. 3.4.1 D, E]. Most of the V-D identified axons were instead active during the rest [fig. 3.2.1 E, F and G, H]. As mice went through training sessions and encountered the aversive stimulus, in the V-D projection more axons gained place-coding property and tiled the belt's length [fig. 3.3.1 B, D]. There was a significant increase in the number of place-coding axons. This increase had a spatial preference for the zone that preceded the airpuff location and occurred as early as the first session of training.

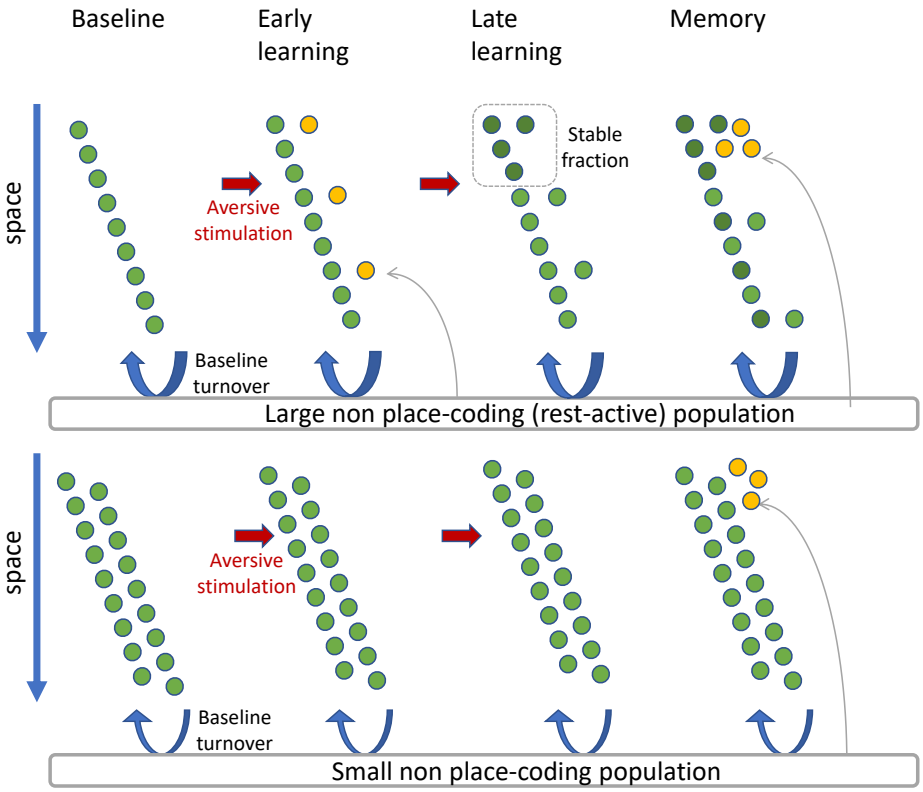

Figure 4.2.1: Dynamics of place maps in the ventral CA3 versus dorsal CA3 - Upper row: in the axons originating from the ventral CA3 a smaller number of cells code the space on the belt and instead a large number are active during the resting states. During learning, the maps undergo a guided change and show an increased representation of the belt in general. In the temporal course of learning, a number of place cells representing the area preceding the aversive experience stabilize. During the retrieval, in the absence of the aversive stimulus, place cells persistently code the important zone on the belt and there are more cells recruited for the representation of this area of the belt. Lower row: the dorsal CA3 maps in general have a higher number of place-coding axons and make up a more precise representation of the space on the belt. The maps however, are less malleable and only gradually represent changes due to the aversive stimulus. After learning, in the absence of the airpuff, new axons code the pre-aversive area, possibly due to the influence of the ventral CA3 or the DG.

Looking at individual axons during each session, a group of previously rest-active axons gained place-coding property and joined the place-coding population (*de novo* axons) [fig. 3.5.1 G]. A subset of these axons stabilized. This stabilized group showed a spatial preference for the zone preceding the airpuff location on the belt, the zone predictive of the aversive stimulus. This phenomenon particularly became significant at the final stages of training [fig. 3.5.2 A]. In the absence of the airpuff, during the probe session a higher number of *de novo* axons joined the place-coding population in the pre-airpuff zone, possibly marking a big difference from the previous day.

The quick deformity in the ventral map upon aversive experience was perhaps due to the influence of amygdalar input reinforcing the CA3 synapses to incorporate space with aversive information. This is in agreement with the reported role of CA3 in rapidly encoding novel information [84, 82]. Upon repeated exposure to the spatial features as well as the airpuff and through the recurrent connectivity, the map stabilized further. In parallel and maybe as a consequence of stabilization, a group of axons were recruited daily into the V-D maps from a large reservoir of rest-active axons. The repetition of experience in the attractor network and influence of the input from amygdala could lead to lasting synaptic changes. This could explain why these axons were added to the group which preferentially encoded the pre-airpuff zone in CA3 maps.

Another possibility is that two parallel processes of learning and retrieval happen inside the CA3 network: the stable fraction is the representation of already encoded features of the environment and general attentive landmarks (allocentric cues) and the *de novo* fraction is encoding the subtle daily changes in the environment, noticed by the animal and overlooked by us [69] in trials with similar conditions.

Eventually, the big changes like presence and absence of the aversive stimulus are similarly and quickly noticed in CA3 by addition of *de novo* axons to the important zone on the belt. Leutgeb et al. 2006 showed that CA3 is capable of rapid encoding of not only spatial information in a new environment, but also encoding of local differences in non-spatial sensory

configuration. CA3 is also capable of associating the non-spatial disparities to the spatial information. This might explain the phenomenon we observed: the stable fraction persistently coded the pre-airpuff zone but the change was then integrated by incorporation of *de novo* fraction into the map during retrieval. CA3 is renowned for immediate incorporation of novel sensory inputs (or the absence of them as in our case) into the otherwise stable place maps [82].

Considering the big reservoir of V-D axons and their population activities during the resting-states, one conjecture could be that resting-state activity orchestrates the recruitment of *de novo* axons and facilitates further stabilization of place-coding axons during the behavioral task. Specifically, the resting activity might stabilize the memory of the learnt features by reactivating the recurrent synapses during states of immobility and consequently preparing more rest-active cells to join the stable population.

On the other hand, throughout the sessions, there was always a richer (in terms of number of place-coding axons) and more precise representation of the belt in the **D-D axonal population**. This is consistent with place-coding properties of dorsal HC [fig. 3.3.1 B, D and fig. 3.4.1 D, E]. In the baseline sessions this axonal population seemed to encode the entire belt regardless of different zones. During the first training session, there were subtle changes (the changes were less dramatic compared to the V-D) in the place maps. But only later, by the end of training, did these changes become significant [fig. 3.4.1 D, E]. The dorsal maps showed a steady level of stability throughout all sessions [fig. 3.5.1 C]. These maps did not exhibit a significant zone specificity. The daily turn-over of *de novo* axons from the smaller rest-active pool of D-D, also does not follow the precise pattern of V-D and pre-airpuff zone specificity and seems to cover a larger part of the belt. Nonetheless, during the memory maintenance phase, the absence of airpuff appeared to be reflected in an increased number of *de novo* axons in the D-D, as the V-D population but with lesser specificity for the pre-airpuff zone [fig. 3.5.2B]. The D-D *de novo* axons almost entirely spared coding the space of the middle zone on the belt.

A smaller effect of zone specificity in D-D axonal projections could be

due to the lack of amygdalar input to this part of the HC [70], but might also be that the effect is masked due to the higher number of place-coding axons in D-D population in every session [fig. 3.3.1D].

Furthermore, the delayed incorporation of aversive effect in the D-D maps compared to the V-D (last training vs. first training), might hint that it takes time for the V-D to exert the effect on the D-D population. Understanding whether this effect in the dorsal CA3 stems from the ventral CA3 or DG would be a subject of future investigations, e.g., silencing the DG input to CA3 and observing the maps in similar behavioral experiments.

Additionally, we did not observe global remapping of the two axonal populations. However, in response to new configuration of sensory cues, rate changes could be a type of remapping specially in CA3, as opposed to the global remapping of cell assemblies. Rate remapping often happens in the dorsal HC in paradigms which proximal cues like the color or the geometry of the arena changes. It was shown that rate remapping is both faster and earlier (almost from the beginning of an experimental trial in a novel environment) in CA3 compared to CA1 [83]. Possible evidence of presence or absence of aversive stimulus with regard to the space might also appear in the form of rate-remapping. Nonetheless, addressing rate-remapping, in an imaging study such as ours, due to the fast spatial traverse of the animal and considering the repeatedly mentioned GCaMP6s calcium dynamics, is not straightforward. If anything, rate remapping might be manifested in the form of amplitude changes. GCaMP6s amplitudes are not a direct translation of airpuffs and the intensities are often variable [26]. This remains to be investigated with ground-truth electrophysiological experiments whether indeed rate-remapping happens.

Furthermore, in contrast to studies delineating lower spatial specificity [64, 111, 120] and larger place fields of ventral HC [71], we did not observe this precision difference when comparing the vector lengths in the V-D CA3 to the D-D population [fig. 3.3.1 I]. The reason could be that the reported differences in precision are not reflected in the axons projecting far away from the cells of origin. It might also be possible that the sub-set cell that give rise to the axons we capture in our imaging study, have differ-

ent spatial-coding properties compared to the previously reported ventral CA3 cells. The electro-physiological recordings that reported the bigger place field size of the ventral CA3 cells were conducted by directly measuring the somata in the ventral CA3.

Briefly, in the context of the HC, perhaps in the dorsal HC, inside the dorsal CA3, the place fields are formed as a result of DG and EC inputs, this also happens in ventral HC functional sub-regions but to a lower degree and in a more sparse fashion. However, as soon as there is an emotional valance introduced to the environment and the role of amygdala kicks off, the ventral sub-regions including ventral CA3 incorporate the additional important sensory information to the place maps by providing more detailed ventral place representation. The longitudinal CA3 projections, might act as an extra player in deformity of the place maps in the dorsal HC and dorsal CA3. The dorsal CA3 under the influence of ventral projections undergoes a delayed deformation and the place maps evolve in a way that the aversion, even transiently is represented. The information, specially the novel experience in the dorsal CA3 is then relayed to the CA1 area and subsequently the downstream neocortical regions for further processing.

Another possible scenario might be that the dorsal CA3 through repeated experience and NMDA dependent synaptic plasticity represents the changes into the place maps with a slower time course compared to the ventral CA3. Most of the cells in the dorsal CA3, however, reinstate the repeating spatial features and elements of the environment. The ventral CA3 projections instead change the place field dynamics through their connections with the dorsal CA1 and its dendrites, something that could be a subject of future investigation.

4.2.2 Encoding of aversive stimulus

In our experiments, since we had a fixed airpuff location, we could not test whether the responses to pure aversion were reflected in the V-D axons. It is also possible that the CA3 neurons encoding the stimulus were not

the same as the ones projecting to the location we were imaging. To effectively tease apart place-coding from pure stimulus coding, experiments with random-location airpuffs are required.

4.2.3 What is the identity of pyramidal cells that the V-D projections originate from?

With our GCaMP6s injections we labeled a large set of CA3 pyramidal cells that cover a range of about 1mm along the septotemporal axis. Whether all ventrally labeled cells project to the dorsal HC or they belong to a specific sub-group of pyramidal cells in the ventral HC, is not known.

Another question would be whether the dorsally projecting cells make other connections along their projection path to the dorsal HC. As explained in chapter 1 there is a topographical relationship between the septotemporal axis of the HC and the EC and neocortical areas [105]. However, due to the anatomical complexity, the CA3 local and general connectivity, despite morphological studies [25, 85, 143, 154], is not very well understood. Although very informative, each study captured only few reconstructed cells in selected levels of septotemporal axis. A global and comprehensive map of CA3 connectivity is still missing which would be a question for connectomics experiments. In addition, the fully reconstructed CA3 axons show extremely ramified axonal trees. How many connection these axons make along their path traversing the septotemporal axis to the dorsal HC, is also not known.

4.2.4 Summary of conclusions and the strengths of this study

Here we demonstrated an additional strength of calcium imaging technique apart from identifying large numbers of neurons across multiple sessions, namely, the ability to disentangle the activity of two **anatomically intermingled projections** of the brain; the axons of CA3 pyramidal cells at two levels of the HC. Doing this was technically impossible by any other existing recording techniques at present. We trained our head-fixed mice to learn and associate *space* and *aversion* by mainly relying on limited sensory

modalities in a given environment.

We demonstrated that the two axonal systems carry different levels of spatial information and exhibit different levels of spatial preference. We report, for the first time, a reservoir of axons in the V-D projection that have high activities during not-running periods and are virtually silent during running when the mice transverse the linear track. These axons were of less abundance in the predominantly place-coding D-D population.

In addition, we could identify the **very thin structure of same axons** across multiple days **experimentally** and track them **computationally**. We could show that the two projections exhibit different degrees of place-coding stability. Finally, we could detect a marked change in the two axonal populations: a change in the coding property of formerly rest-active fraction to coding the space. This study not only sheds light on information content of two main communication routes inside the HC but also highlights broader implications of two-photon imaging technique for studying projections in the brain and investigating the neural correlates of behavior in them.

Acknowledgments

First and foremost, I would like to express my deepest gratitude to my supervisor Prof. Dr. Heinz Beck for believing in me and giving me the opportunity to do my PhD in his lab. Needless to say, without his scientific advice and continuous support, this work would not have been possible. His trust and positive attitude towards young students such as myself, his availability and generosity in combination with his scientific rigour has been exemplary throughout these years. His way of winning people's respect by being unbelievably humble but also providing advice and guiding them through problems has been a life lesson for me. I am grateful for having experienced that despite thick and thin I have been through during my graduate research.

I am thankful and honored to have Pro. Dr. Walter Witke, Prof. Dr. Von der Emde and Prof. Dr. Evi Kostenis as members of my thesis committee.

Next, I would like to thank my companion, colleague and friend, Martin Pofahl. We spent nearly a decade worth of ups and downs together for building the two-photon technique in the lab and conducting our respective projects. Many moments of frustration, and of course joy has made our relationship exceptional and beyond merely teammates and work colleagues. He has had immense intellectual contribution to this project for which I am ever grateful.

I am particularly grateful to Margit Reitze for handling lots of administrative riddles and for putting order to situations that could have been chaotic otherwise, specially during the long process of establishment.

I am sincerely grateful to the late Klaus Granitza for his enormous assistance in building the many pieces of our experimental rig and for his craftsmanship that we treasure and whose loss anguished our hearts. We did not have time to thank him properly but he is and will be dearly missed and his legacy will live in our minds and surely in our two-photon rigs.

I would like to thank Dr. Fatemeh Kamali and Dr. Kurtulus Gölcük for their advice and scientific contribution to this thesis. I would like to thank my friend Dilek Mercan, whose energy and songs cheered me up so many

times, specially during the final stages of writing this dissertation. Our many shared working weekends and official holidays has been less lonely and definitely more joyful with her!

I would like to thank all the wonderful people that are and were in the lab who added to the warmth and joy of our working environment. Repeatedly I heard from others that we have an exceptional synergy and atmosphere in our working environment. To this end, I would like to thank, Dr. Laura Ewell, Dr. Thoralf Opitz, Dr. Tony Kelly, Nicola Masala, Pedro Royero, Daniel Müller, Micheala Barboni, Suncana Novosel, Paunica Giesler, Sabrina Minacapilli, Nicole Schönfelder and Kristian Reichelt.

I would like to thank my dear sister Sarah Schmidt whom I consider my extended family in Germany and with whom I have had the chance of sharing deep aspects of 'humanity', intellectual discovery and understanding. Getting to know her was one of the luckiest incidences of my PhD. We celebrated the unity and continuum of humanity and ridiculed the artificial borders over several cups of coffee.

Finally, I would like to thank my family, my parents and my sister for supporting me from near and far and for respecting my decisions without hesitation and for their enduring of long periods of separation and absence. I would like to thank my partner Amir for his immense patience and understanding as he walked by my side and encouraged me to continue when I felt otherwise. He touched the insufferable moments of disappointment that I experienced and encouraged me to go on!

Lastly, I would like to thank my precious brother, Nader, who has been a source of inspiration and motivation for me. He continuously gave me constructive inputs throughout the course of writing of this thesis and to whose intellect I owe big time.

References

[1] Farhan Ali and Alex C Kwan. Interpreting in vivo calcium signals from neuronal cell bodies, axons, and dendrites: a review. *Neurophotonics*, 7(1):011402, 2019.

[2] David Amaral and Pierre Lavenex. Hippocampal neuroanatomy. 2007.

[3] David G Amaral. Hippocampal formation. *The rat nervous system*, pages 443–493, 1995.

[4] David G Amaral and Judith A Dent. Development of the mossy fibers of the dentate gyrus: I. a light and electron microscopic study of the mossy fibers and their expansions. *Journal of Comparative Neurology*, 195(1):51–86, 1981.

[5] David G Amaral and J Kurz. An analysis of the origins of the cholinergic and noncholinergic septal projections to the hippocampal formation of the rat. *Journal of Comparative Neurology*, 240(1):37–59, 1985.

[6] David G Amaral and JL Price. Amygdalo-cortical projections in the monkey (macaca fascicularis). *Journal of Comparative Neurology*, 230(4):465–496, 1984.

[7] David G Amaral and Menno P Witter. The three-dimensional organization of the hippocampal formation: a review of anatomical data. *Neuroscience*, 31(3):571–591, 1989.

[8] Stephan G Anagnostaras, Stephen Maren, and Michael S Fanselow. Temporally graded retrograde amnesia of contextual fear after hippocampal damage in rats: within-subjects examination. *Journal of Neuroscience*, 19(3):1106–1114, 1999.

[9] Per Andersen. Organization of hippocampal neurons and their interconnections. In *The hippocampus*, pages 155–175. Springer, 1975.

[10] Tobias Bast, Iain A Wilson, Menno P Witter, and Richard GM Morris. From rapid place learning to behavioral performance: a key role for the intermediate hippocampus. *PLoS Biol*, 7(4):e1000089, 2009.

[11] Mary Behan and Lewis B Haberly. Intrinsic and efferent connections of the endopiriform nucleus in rat. *Journal of Comparative Neurology*, 408(4):532–548, 1999.

[12] Antoine Besnard, Yuan Gao, Michael TaeWoo Kim, Hannah Twarkowski, Alexander Keith Reed, Tomer Langberg, Wendy Feng, Xiangmin Xu, Dieter Saur, Larry S Zweifel, et al. Dorsolateral septum somatostatin interneurons gate mobility to calibrate context-specific behavioral fear responses. *Nature neuroscience*, 22 (3):436–446, 2019.

[13] Antoine Besnard, Samara M Miller, and Amar Sahay. Distinct dorsal and ventral hippocampal ca3 outputs govern contextual fear discrimination. *Cell reports*, 30(7):2360–2373, 2020.

[14] TW Blackstad, K Brink, J Hem, and B June. Distribution of hippocampal mossy fibers in the rat. an experimental study with silver impregnation methods. *Journal of Comparative Neurology*, 138(4): 433–449, 1970.

[15] Robert J Blanchard and D Caroline Blanchard. Crouching as an index of fear. *Journal of comparative and physiological psychology*, 67 (3):370, 1969.

[16] Daniel J Bonthius, Ross McKim, Lindsey Koele, Harb Harb, Bahri Karacay, Jo Mahoney, and Nicholas J Pantazis. Use of frozen sections to determine neuronal number in the murine hippocampus and neocortex using the optical disector and optical fractionator. *Brain research protocols*, 14(1):45–57, 2004.

[17] Mark E Bouton and Robert C Bolles. Conditioned fear assessed by freezing and by the suppression of three different baselines. *Animal learning & behavior*, 8(3):429–434, 1980.

[18] Gerard Joey Broussard, Yajie Liang, Marina Fridman, Elizabeth K Unger, Guanghan Meng, Xian Xiao, Na Ji, Leopoldo Petreanu, and Lin Tian. In vivo measurement of afferent activity with axon-specific calcium imaging. *Nature neuroscience*, 21(9):1272–1280, 2018.

[19] Vegard H Brun, Mona K Otnæss, Sturla Molden, Hill-Aina Steffenach, Menno P Witter, May-Britt Moser, and Edvard I Moser. Place cells and place recognition maintained by direct entorhinal-hippocampal circuitry. *Science*, 296(5576):2243–2246, 2002.

[20] PAUL S Buckmaster, BW Strowbridge, and PHILIP A Schwartzkroin. A comparison of rat hippocampal mossy cells and ca3c pyramidal cells. *Journal of Neurophysiology*, 70(4): 1281–1299, 1993.

[21] Neil Burgess, Eleanor A Maguire, and John O'Keefe. The human hippocampus and spatial and episodic memory. *Neuron*, 35(4): 625–641, 2002.

[22] György Buzsáki. Hippocampal sharp wave-ripple: A cognitive biomarker for episodic memory and planning. *Hippocampus*, 25 (10):1073–1188, 2015.

[23] György Buzsáki and David Tingley. Space and time: The hippocampus as a sequence generator. *Trends in cognitive sciences*, 22 (10):853–869, 2018.

[24] György Buzsáki, Cornelius H Vanderwolf, et al. Cellular bases of hippocampal eeg in the behaving rat. *Brain Research Reviews*, 6(2): 139–171, 1983.

[25] Robert C Cannon, DA Turner, GK Pyapali, and HV Wheal. An on-line archive of reconstructed hippocampal neurons. *Journal of neuroscience methods*, 84(1-2):49–54, 1998.

[26] Tsai-Wen Chen, Trevor J Wardill, Yi Sun, Stefan R Pulver, Sabine L Renninger, Amy Baohan, Eric R Schreiter, Rex A Kerr, Michael B Orger, Vivek Jayaraman, et al. Ultrasensitive fluorescent proteins for imaging neuronal activity. *Nature*, 499(7458):295–300, 2013.

[27] Enrico Cherubini and Richard Miles Miles. The ca3 region of the hippocampus: how is it? what is it for? how does it do it? *Frontiers in cellular neuroscience*, 9:19, 2015.

[28] Brenda J Claiborne, David G Amaral, and W Maxwell Cowan. A light and electron microscopic analysis of the mossy fibers of the rat dentate gyrus. *Journal of comparative neurology*, 246(4):435–458, 1986.

[29] Charles L Cox, Winfried Denk, David W Tank, and Karel Svoboda. Action potentials reliably invade axonal arbors of rat neocortical neurons. *Proceedings of the National Academy of Sciences*, 97(17): 9724–9728, 2000.

[30] Jozsef Csicsvari, Hajime Hirase, Akira Mamiya, and György Buzsáki. Ensemble patterns of hippocampal ca3-ca1 neurons during sharp wave–associated population events. *Neuron*, 28(2):585–594, 2000.

[31] Nathan B Danielson, Patrick Kaifosh, Jeffrey D Zaremba, Matthew Lovett-Barron, Joseph Tsai, Christine A Denny, Elizabeth M Balough, Alexander R Goldberg, Liam J Drew, René Hen, et al. Distinct contribution of adult-born hippocampal granule cells to context encoding. *Neuron*, 90(1):101–112, 2016.

[32] Peter Dayan. Improving generalization for temporal difference learning: The successor representation. *Neural Computation*, 5(4): 613–624, 1993.

[33] Steven Demeter, Douglas L Rosene, and Gary W van Hoesen. Interhemispheric pathways of the hippocampal formation, presubiculum, and entorhinal and posterior parahippocampal cortices in the rhesus monkey: the structure and organization of the hippocampal commissures. *Journal of comparative neurology*, 233(1): 30–47, 1985.

[34] Viet H Do, Carlo O Martinez, Joe L Martinez Jr, and Brian E Derrick. Long-term potentiation in direct perforant path projections to the hippocampal ca3 region in vivo. *Journal of Neurophysiology*, 87(2):669–678, 2002.

[35] Daniel A Dombeck, Christopher D Harvey, Lin Tian, Loren L Looger, and David W Tank. Functional imaging of hippocampal place cells at cellular resolution during virtual navigation. *Nature neuroscience*, 13(11):1433–1440, 2010.

[36] Can Dong and Mark Sheffield. Distinct place cell dynamics in ca1 and ca3 encode experience in new contexts. *bioRxiv*, 2020.

[37] Richard O Duda and Peter E Hart. Use of the hough transformation to detect lines and curves in pictures. *Communications of the ACM*, 15(1):11–15, 1972.

[38] David Dupret, Joseph O'neill, Barty Pleydell-Bouverie, and Jozsef Csicsvari. The reorganization and reactivation of hippocampal maps predict spatial memory performance. *Nature neuroscience*, 13 (8):995, 2010.

[39] AD Ekstrom, J Meltzer, BL McNaughton, and CA Barnes. Nmda receptor antagonism blocks experience-dependent expansion of hippocampal "place fields". *Neuron*, 31(4):631–638, 2001.

[40] Michael S Fanselow and Hong-Wei Dong. Are the dorsal and ventral hippocampus functionally distinct structures? *Neuron*, 65(1): 7–19, 2010.

[41] Michael S Fanselow and Andrew M Poulos. The neuroscience of mammalian associative learning. *Annu. Rev. Psychol.*, 56:207–234, 2005.

[42] Paul W Frankland, Vincenzo Cestari, Robert K Filipkowski, Robert J McDonald, and Alcino J Silva. The dorsal hippocampus is essential for context discrimination but not for contextual conditioning. *Behavioral neuroscience*, 112(4):863, 1998.

[43] Tamás F Freund and Miklós Antal. Gaba-containing neurons in the septum control inhibitory interneurons in the hippocampus. *Nature*, 336(6195):170–173, 1988.

[44] R Fricke and WM Cowan. An autoradiographic study of the commissural and ipsilateral hippocampo-dentate projections in the adult rat. *Journal of Comparative Neurology*, 181(2):253–269, 1978.

[45] Michael Frotscher and Jens Zimmer. Commissural fibers terminate on non-pyramidal neurons in the guinea pig hippocampus—a combined golgi/em degeneration study. *Brain research*, 265(2): 289–293, 1983.

[46] FrankB Gaarskjaer. The organization and development of the hippocampal mossy fiber system. *Brain Research Reviews*, 11(4):335–357, 1986.

[47] Ronald PA Gaykema, Paul GM Luiten, Csaba Nyakas, and Jörg Traber. Cortical projection patterns of the medial septum-diagonal band complex. *Journal of Comparative Neurology*, 293(1):103–124, 1990.

[48] Lindsey L Glickfeld, Mark L Andermann, Vincent Bonin, and R Clay Reid. Cortico-cortical projections in mouse visual cortex are functionally target specific. *Nature neuroscience*, 16(2):219–226, 2013.

[49] David S Greenberg and Jason ND Kerr. Automated correction of fast motion artifacts for two-photon imaging of awake animals. *Journal of neuroscience methods*, 176(1):1–15, 2009.

[50] AI Gulyás, TJ Görcs, and TF Freund. Innervation of different peptide-containing neurons in the hippocampus by gabaergic septal afferents. *Neuroscience*, 37(1):31–44, 1990.

[51] Attila I Gulyás, N Hajos, I Katona, and TF Freund. Interneurons are the local targets of hippocampal inhibitory cells which project to the medial septum. *European Journal of Neuroscience*, 17(9):1861–1872, 2003.

[52] Zengcai V Guo, S Andrew Hires, Nuo Li, Daniel H O'Connor, Takaki Komiyama, Eran Ophir, Daniel Huber, Claudia Bonardi, Karin Morandell, Diego Gutnisky, et al. Procedures for behavioral experiments in head-fixed mice. *PloS one*, 9(2):e88678, 2014.

[53] Michael E Hasselmo, Eric Schnell, and Edi Barkai. Dynamics of learning and recall at excitatory recurrent synapses and cholinergic modulation in rat hippocampal region ca3. *Journal of Neuroscience*, 15(7):5249–5262, 1995.

[54] Fritjof Helmchen and Winfried Denk. Deep tissue two-photon microscopy. *Nature methods*, 2(12):932–940, 2005.

[55] Miles Herkenham. The connections of the nucleus reuniens thalami: Evidence for a direct thalamo-hippocampal pathway in the rat. *Journal of Comparative Neurology*, 177(4):589–609, 1978.

[56] Paul VC Hough. Method and means for recognizing complex patterns, December 18 1962. US Patent 3,069,654.

[57] Marc W Howard and Howard Eichenbaum. Time and space in the hippocampus. *Brain research*, 1621:345–354, 2015.

[58] Michael R Hunsaker and Raymond P Kesner. Dissociations across the dorsal–ventral axis of ca3 and ca1 for encoding and retrieval of contextual and auditory-cued fear. *Neurobiology of learning and memory*, 89(1):61–69, 2008.

[59] Michael R Hunsaker, Graham G Mooy, Jesse S Swift, and Raymond P Kesner. Dissociations of the medial and lateral perforant path projections into dorsal dg, ca3, and ca1 for spatial and nonspatial (visual object) information processing. *Behavioral neuroscience*, 121(4):742, 2007.

[60] Norio Ishizuka, Janet Weber, and David G Amaral. Organization of intrahippocampal projections originating from ca3 pyramidal cells in the rat. *Journal of comparative neurology*, 295(4):580–623, 1990.

[61] Norio Ishizuka, W Maxwell Cowan, and David G Amaral. A quantitative analysis of the dendritic organization of pyramidal cells in the rat hippocampus. *Journal of Comparative Neurology*, 362(1): 17–45, 1995.

[62] Taylor Jerman, Raymond P Kesner, and Michael R Hunsaker. Disconnection analysis of ca3 and dg in mediating encoding but not retrieval in a spatial maze learning task. *Learning & Memory*, 13 (4):458–464, 2006.

[63] Min W Jung, Sidney I Wiener, and Bruce L McNaughton. Comparison of spatial firing characteristics of units in dorsal and ventral hippocampus of the rat. *Journal of Neuroscience*, 14(12):7347–7356, 1994.

[64] MW Jung and BL McNaughton. Spatial selectivity of unit activity in the hippocampal granular layer. *Hippocampus*, 3(2):165–182, 1993.

[65] Eric R Kandel, James H Schwartz, Thomas M Jessell, Steven Siegelbaum, A James Hudspeth, and Sarah Mack. *Principles of neural science*, volume 4. McGraw-hill New York, 2000.

[66] Raymond P Kesner. Behavioral functions of the ca3 subregion of the hippocampus. *Learning & memory*, 14(11):771–781, 2007.

[67] Mazen A Kheirbek, Liam J Drew, Nesha S Burghardt, Daniel O Costantini, Lindsay Tannenholz, Susanne E Ahmari, Hongkui Zeng, André A Fenton, and René Hen. Differential control of learning and anxiety along the dorsoventral axis of the dentate gyrus. *Neuron*, 77(5):955–968, 2013.

[68] Jeansok J Kim, Richard A Rison, and Michael S Fanselow. Effects of amygdala, hippocampus, and periaqueductal gray lesions on short- and long-term contextual fear. *Behavioral neuroscience*, 107(6): 1093, 1993.

[69] Nathaniel R Kinsky, David W Sullivan, William Mau, Michael E Hasselmo, and Howard B Eichenbaum. Hippocampal place fields maintain a coherent and flexible map across long timescales. *Current Biology*, 28(22):3578–3588, 2018.

[70] Toshiro Kishi, Toshiko Tsumori, Shigefumi Yokota, and Yukihiko Yasui. Topographical projection from the hippocampal formation to the amygdala: a combined anterograde and retrograde tracing study in the rat. *Journal of Comparative Neurology*, 496(3):349–368, 2006.

[71] Kirsten Brun Kjelstrup, Trygve Solstad, Vegard Heimly Brun, Torkel Hafting, Stefan Leutgeb, Menno P Witter, Edvard I Moser, and May-Britt Moser. Finite scale of spatial representation in the hippocampus. *Science*, 321(5885):140–143, 2008.

[72] Kirsten G Kjelstrup, Frode A Tuvnes, Hill-Aina Steffenach, Robert Murison, Edvard I Moser, and May-Britt Moser. Reduced fear expression after lesions of the ventral hippocampus. *Proceedings of the National Academy of Sciences*, 99(16):10825–10830, 2002.

[73] Helmut J Koester and Daniel Johnston. Target cell-dependent normalization of transmitter release at neocortical synapses. *Science*, 308(5723):863–866, 2005.

[74] Helmut J Koester and Bert Sakmann. Calcium dynamics associated with action potentials in single nerve terminals of pyramidal cells in layer 2/3 of the young rat neocortex. *The Journal of physiology*, 529 (3):625–646, 2000.

[75] Christer Köhler, Victoria Chan-Palay, and Jang-Yen Wu. Septal neurons containing glutamic acid decarboxylase immunoreactivity

project to the hippocampal region in the rat brain. *Anatomy and embryology*, 169(1):41–44, 1984.

[76] M Lauer and D Senitz. Dendritic excrescences seem to characterize hippocampal ca3 pyramidal neurons in humans. *Journal of neural transmission*, 113(10):1469–1475, 2006.

[77] Christian R Lee and David J Margolis. Pupil dynamics reflect behavioral choice and learning in a go/nogo tactile decision-making task in mice. *Frontiers in behavioral neuroscience*, 10:200, 2016.

[78] Inah Lee and Raymond P Kesner. Differential contribution of nmda receptors in hippocampal subregions to spatial working memory. *Nature neuroscience*, 5(2):162–168, 2002.

[79] Inah Lee and Raymond P Kesner. Differential contributions of dorsal hippocampal subregions to memory acquisition and retrieval in contextual fear-conditioning. *Hippocampus*, 14(3):301–310, 2004.

[80] Inah Lee, Geeta Rao, and James J Knierim. A double dissociation between hippocampal subfields: differential time course of ca3 and ca1 place cells for processing changed environments. *Neuron*, 42 (5):803–815, 2004.

[81] Sang Wan Lee, John P O'Doherty, and Shinsuke Shimojo. Neural computations mediating one-shot learning in the human brain. *PLoS Biol*, 13(4):e1002137, 2015.

[82] Stefan Leutgeb and Jill K Leutgeb. Pattern separation, pattern completion, and new neuronal codes within a continuous ca3 map. *Learning & memory*, 14(11):745–757, 2007.

[83] Stefan Leutgeb, Jill K Leutgeb, Carol A Barnes, Edvard I Moser, Bruce L McNaughton, and May-Britt Moser. Independent codes for spatial and episodic memory in hippocampal neuronal ensembles. *Science*, 309(5734):619–623, 2005.

[84] Stefan Leutgeb, Jill K Leutgeb, Edvard I Moser, and May-Britt Moser. Fast rate coding in hippocampal ca3 cell ensembles. *Hippocampus*, 16(9):765–774, 2006.

[85] X-G Li, P Somogyi, A Ylinen, and G Buzsáki. The hippocampal ca3 network: an in vivo intracellular labeling study. *Journal of comparative neurology*, 339(2):181–208, 1994.

[86] Maria Llorens-Martín, Lidia Blazquez-Llorca, Ruth Benavides-Piccione, Alberto Rabano, Felix Hernandez, Jesus Avila, and Javier DeFelipe. Selective alterations of neurons and circuits related to early memory loss in alzheimer's disease. *Frontiers in neuroanatomy*, 8:38, 2014.

[87] Matthew Lovett-Barron, Patrick Kaifosh, Mazen A Kheirbek, Nathan Danielson, Jeffrey D Zaremba, Thomas R Reardon, Gergely F Turi, René Hen, Boris V Zemelman, and Attila Losonczy. Dendritic inhibition in the hippocampus supports fear learning. *Science*, 343(6173):857–863, 2014.

[88] Jeffrey C Magee and Christine Grienberger. Synaptic plasticity forms and functions. *Annual Review of Neuroscience*, 43, 2020.

[89] William J Mahoney and John JB Ayres. One-trial simultaneous and backward fear conditioning as reflected in conditioned suppression of licking in rats. *Animal Learning & Behavior*, 4(4):357–362, 1976.

[90] Alexander Mathis, Pranav Mamidanna, Kevin M Cury, Taiga Abe, Venkatesh N Murthy, Mackenzie Weygandt Mathis, and Matthias Bethge. Deeplabcut: markerless pose estimation of user-defined body parts with deep learning. *Nature neuroscience*, 21(9):1281–1289, 2018.

[91] Ellen M McGlinchey and Gary Aston-Jones. Dorsal hippocampus drives context-induced cocaine seeking via inputs to lateral septum. *Neuropsychopharmacology*, 43(5):987–1000, 2018.

[92] Bruce L McNaughton and Richard GM Morris. Hippocampal synaptic enhancement and information storage within a distributed memory system. *Trends in neurosciences*, 10(10):408–415, 1987.

[93] Bruce L McNaughton, Carol A Barnes, and JJEBR O'Keefe. The contributions of position, direction, and velocity to single unit activity in the hippocampus of freely-moving rats. *Experimental brain research*, 52(1):41–49, 1983.

[94] Mayank R Mehta, Michael C Quirk, and Matthew A Wilson. Experience-dependent asymmetric shape of hippocampal receptive fields. *Neuron*, 25(3):707–715, 2000.

[95] Richard GM Morris, Paul Garrud, JNP al Rawlins, and John O'Keefe. Place navigation impaired in rats with hippocampal lesions. *Nature*, 297(5868):681–683, 1982.

[96] May-Britt Moser and Edvard I Moser. Distributed encoding and retrieval of spatial memory in the hippocampus. *Journal of Neuroscience*, 18(18):7535–7542, 1998.

[97] Robert U Muller, John L Kubie, and James B Ranck. Spatial firing patterns of hippocampal complex-spike cells in a fixed environment. *Journal of Neuroscience*, 7(7):1935–1950, 1987.

[98] Lynn Nadel and Jeffrey Willner. Context and conditioning: A place for space. *Physiological Psychology*, 8(2):218–228, 1980.

[99] Lynn Nadel, Jeffrey Willner, and Elizabeth M Kurz. Cognitive maps and environmental context. *Context and learning*, 385406, 1985.

[100] Kazu Nakazawa, Michael C Quirk, Raymond A Chitwood, Masahiko Watanabe, Mark F Yeckel, Linus D Sun, Akira Kato, Candice A Carr, Daniel Johnston, Matthew A Wilson, et al. Requirement for hippocampal ca3 nmda receptors in associative memory recall. *science*, 297(5579):211–218, 2002.

[101] John O'Keefe and Jonathan Dostrovsky. The hippocampus as a spatial map: Preliminary evidence from unit activity in the freely-moving rat. *Brain research*, 1971.

[102] John O'keefe and Lynn Nadel. *The hippocampus as a cognitive map*. Oxford: Clarendon Press, 1978.

[103] John O'Keefe and Michael L Recce. Phase relationship between hippocampal place units and the eeg theta rhythm. *Hippocampus*, 3(3):317–330, 1993.

[104] Wei-Xing Pan and Neil McNaughton. The supramammillary area: its organization, functions and relationship to the hippocampus. *Progress in neurobiology*, 74(3):127–166, 2004.

[105] Jagdish Patel, Erik W Schomburg, Antal Berényi, Shigeyoshi Fujisawa, and György Buzsáki. Local generation and propagation of ripples along the septotemporal axis of the hippocampus. *Journal of Neuroscience*, 33(43):17029–17041, 2013.

[106] Leopoldo Petreanu, Diego A Gutnisky, Daniel Huber, Ning-long Xu, Dan H O'Connor, Lin Tian, Loren Looger, and Karel Svoboda. Activity in motor–sensory projections reveals distributed coding in somatosensation. *Nature*, 489(7415):299–303, 2012.

[107] Maria Pikkarainen, Seppo Rönkkö, Vesa Savander, Ricardo Insausti, and Asla Pitkänen. Projections from the lateral, basal, and accessory basal nuclei of the amygdala to the hippocampal formation in rat. *Journal of Comparative Neurology*, 403(2):229–260, 1999.

[108] Asla Pitkänen, Maria Pikkarainen, Nina Nurminen, and Aarne Ylinen. Reciprocal connections between the amygdala and the hippocampal formation, perirhinal cortex, and postrhinal cortex in rat: a review. *Annals of the new York Academy of Sciences*, 911(1):369–391, 2000.

[109] Eftychios A Pnevmatikakis and Andrea Giovannucci. Normcorre: An online algorithm for piecewise rigid motion correction of calcium imaging data. *Journal of neuroscience methods*, 291:83–94, 2017.

[110] Eftychios A Pnevmatikakis, Daniel Soudry, Yuanjun Gao, Timothy A Machado, Josh Merel, David Pfau, Thomas Reardon, Yu Mu, Clay Lacefield, Weijian Yang, et al. Simultaneous denoising, deconvolution, and demixing of calcium imaging data. *Neuron*, 89 (2):285–299, 2016.

[111] Bruno Poucet, Catherine Thinus-Blanc, and Robert U Muller. Place cells in the ventral hippocampus of rats. *Neuroreport: An International Journal for the Rapid Communication of Research in Neuroscience*, 1994.

[112] Priyamvada Rajasethupathy, Sethuraman Sankaran, James H Marshel, Christina K Kim, Emily Ferenczi, Soo Yeun Lee, Andre Berndt, Charu Ramakrishnan, Anna Jaffe, Maisie Lo, et al. Projections from neocortex mediate top-down control of memory retrieval. *Nature*, 526(7575):653–659, 2015.

[113] Santiago Ramon y Cajal. Histologie du système nerveux de l'homme et des vertébrés. *Maloine, Paris*, 2:153–173, 1911.

[114] Jacob Reimer, Emmanouil Froudarakis, Cathryn R Cadwell, Dimitri Yatsenko, George H Denfield, and Andreas S Tolias. Pupil fluc-

tuations track fast switching of cortical states during quiet wakefulness. *Neuron*, 84(2):355–362, 2014.

[115] PY Risold and LW Swanson. Connections of the rat lateral septal complex. *Brain research reviews*, 24(2-3):115–195, 1997.

[116] Kathleen S Rockland. Axon collaterals and brain states. *Frontiers in systems neuroscience*, 12:32, 2018.

[117] Jason L Rogers and Raymond P Kesner. Cholinergic modulation of the hippocampus during encoding and retrieval. *Neurobiology of learning and memory*, 80(3):332–342, 2003.

[118] Jason L Rogers and Raymond P Kesner. Cholinergic modulation of the hippocampus during encoding and retrieval of tone/shock-induced fear conditioning. *Learning & Memory*, 11(1):102–107, 2004.

[119] Edmund T Rolls. Functions of neuronal networks in the hippocampus and neocortex in memory. In *Neural models of plasticity*, pages 240–265. Elsevier, 1989.

[120] Sébastien Royer, Anton Sirota, Jagdish Patel, and György Buzsáki. Distinct representations and theta dynamics in dorsal and ventral hippocampus. *Journal of Neuroscience*, 30(5):1777–1787, 2010.

[121] Jerry W Rudy and Randall C O'Reilly. Conjunctive representations, the hippocampus, and contextual fear conditioning. *Cognitive, Affective, & Behavioral Neuroscience*, 1(1):66–82, 2001.

[122] JW Rudy, NC Huff, and P Matus-Amat. Understanding contextual fear conditioning: insights from a two-process model. *Neuroscience & Biobehavioral Reviews*, 28(7):675–685, 2004.

[123] Sarah Ruediger, Dominique Spirig, Flavio Donato, and Pico Caroni. Goal-oriented searching mediated by ventral hippocampus early in trial-and-error learning. *Nature neuroscience*, 15(11):1563–1571, 2012.

[124] Josef HLP Sadowski, Matthew W Jones, and Jack R Mellor. Sharp-wave ripples orchestrate the induction of synaptic plasticity during reactivation of place cell firing patterns in the hippocampus. *Cell reports*, 14(8):1916–1929, 2016.

[125] HELEN E Scharfman. Evidence from simultaneous intracellular recordings in rat hippocampal slices that area ca3 pyramidal cells innervate dentate hilar mossy cells. *Journal of Neurophysiology*, 72 (5):2167–2180, 1994.

[126] Hannsjörg Schröder, Natasha Moser, and Stefan Huggenberger. The mouse hippocampus. In *Neuroanatomy of the Mouse*, pages 267–288. Springer, 2020.

[127] Wolfram Schultz, Peter Dayan, and P Read Montague. A neural substrate of prediction and reward. *Science*, 275(5306):1593–1599, 1997.

[128] Gordon MG Shepherd and Kristen M Harris. Three-dimensional structure and composition of ca3→ ca1 axons in rat hippocampal slices: implications for presynaptic connectivity and compartmentalization. *Journal of Neuroscience*, 18(20):8300–8310, 1998.

[129] Hideshi Shibata. Direct projections from the anterior thalamic nuclei to the retrohippocampal region in the rat. *Journal of Comparative Neurology*, 337(3):431–445, 1993.

[130] Attila Sik, Aarne Ylinen, Markku Penttonen, and Gyorgy Buzsaki. Inhibitory ca1-ca3-hilar region feedback in the hippocampus. *Science*, 265(5179):1722–1724, 1994.

[131] Burrhus Frederic Skinner. The behavior of organisms: an experimental analysis. appleton-century, 1938.

[132] KE Sorra and Kristen M Harris. Occurrence and three-dimensional structure of multiple synapses between individual radiatum axons and their target pyramidal cells in hippocampal area ca1. *Journal of Neuroscience*, 13(9):3736–3748, 1993.

[133] Marielena Sosa, Anna K Gillespie, and Loren M Frank. Neural activity patterns underlying spatial coding in the hippocampus. *Behavioral Neuroscience of Learning and Memory*, pages 43–100, 2016.

[134] Kimberly L Stachenfeld, Matthew M Botvinick, and Samuel J Gershman. The hippocampus as a predictive map. *Nature neuroscience*, 20(11):1643, 2017.

[135] Bryan A Strange, Menno P Witter, Ed S Lein, and Edvard I Moser. Functional organization of the hippocampal longitudinal axis. *Nature Reviews Neuroscience*, 15(10):655–669, 2014.

[136] LW Swanson, JM Wyss, and WM Cowan. An autoradiographic study of the organization of intrahippocampal association pathways in the rat. *Journal of comparative neurology*, 181(4):681–715, 1978.

[137] LW Swanson, PE Sawchenko, and WM Cowan. Evidence that the commissural, associational and septal projections of the regio inferior of the hippocampus arise from the same neurons. *Brain research*, 197(1):207–212, 1980.

[138] Carol L Thompson, Sayan D Pathak, Andreas Jeromin, Lydia L Ng, Cameron R MacPherson, Marty T Mortrud, Allison Cusick, Zackery L Riley, Susan M Sunkin, Amy Bernard, et al. Genomic anatomy of the hippocampus. *Neuron*, 60(6):1010–1021, 2008.

[139] Edward L Thorndike. Animal intelligence: an experimental study of the associative processes in animals. *The Psychological Review: Monograph Supplements*, 2(4):i, 1898.

[140] Edward Lee Thorndike. *The elements of psychology*. AG Seiler, 1905.

[141] Lin Tian, S Andrew Hires, Tianyi Mao, Daniel Huber, M Eugenia Chiappe, Sreekanth H Chalasani, Leopoldo Petreanu, Jasper Akerboom, Sean A McKinney, Eric R Schreiter, et al. Imaging neural activity in worms, flies and mice with improved gcamp calcium indicators. *Nature methods*, 6(12):875–881, 2009.

[142] E Tulving. Elements of episodic memory. clarendon, 1983.

[143] DA Turner, X-G Li, GK Pyapali, A Ylinen, and G Buzsaki. Morphometric and electrical properties of reconstructed hippocampal ca3 neurons recorded in vivo. *Journal of Comparative Neurology*, 356 (4):580–594, 1995.

[144] David R Vago, Adam Bevan, and Raymond P Kesner. The role of the direct perforant path input to the ca1 subregion of the dorsal hippocampus in memory retention and retrieval. *Hippocampus*, 17 (10):977–987, 2007.

[145] Thomas van Groen, Pasi Miettinen, and Inga Kadish. The entorhinal cortex of the mouse: organization of the projection to the hippocampal formation. *Hippocampus*, 13(1):133–149, 2003.

[146] Douglas Wahlsten. *Mouse behavioral testing: how to use mice in behavioral neuroscience*. Academic Press, 2010.

[147] Scoville Wb et al. Loss of recent memory after bilateral hippocampal lesions. *Journal of Neurology, Neurosurgery, and Psychiatry*, 20 (1):11–21, 1957.

[148] Lesnick E Westrum and Theodor W Blackstad. An electron microscopic study of the stratum radiatum of the rat hippocampus (regio superior, ca 1) with particular emphasis on synaptology. *Journal of Comparative Neurology*, 119(3):281–309, 1962.

[149] Menno P Witter. Connections of the subiculum of the rat: topography in relation to columnar and laminar organization. *Behavioural brain research*, 174(2):251–264, 2006.

[150] Menno P Witter. Intrinsic and extrinsic wiring of ca3: indications for connectional heterogeneity. *Learning & memory*, 14(11):705–713, 2007.

[151] Menno P Witter. The perforant path: projections from the entorhinal cortex to the dentate gyrus. *Progress in brain research*, 163:43–61, 2007.

[152] Menno P Witter et al. Organization of the entorhinal-hippocampal system: a review of current anatomical data. *HIPPOCAMPUS-NEW YORK-CHURCHILL LIVINGSTONE-*, 3:33–33, 1993.

[153] MP Witter, GW Van Hoesen, and David G Amaral. Topographical organization of the entorhinal projection to the dentate gyrus of the monkey. *Journal of Neuroscience*, 9(1):216–228, 1989.

[154] Lucia Wittner, Darrell A Henze, László Záborszky, and György Buzsáki. Three-dimensional reconstruction of the axon arbor of a ca3 pyramidal cell recorded and filled in vivo. *Brain Structure and Function*, 212(1):75–83, 2007.

[155] Floris G Wouterlood, Enrique Saldana, and Menno P Witter. Projection from the nucleus reuniens thalami to the hippocampal region: light and electron microscopic tracing study in the rat with the anterograde tracer phaseolus vulgaris-leucoagglutinin. *Journal of Comparative Neurology*, 296(2):179–203, 1990.

[156] Mariko Yamano and Paul GM Luiten. Direct synaptic contacts of medial septal efferents with somatostatin immunoreactive neurons in the rat hippocampus. *Brain research bulletin*, 22(6):993–1001, 1989.

[157] Mark F Yeckel and Theodore W Berger. Feedforward excitation of the hippocampus by afferents from the entorhinal cortex: redefinition of the role of the trisynaptic pathway. *Proceedings of the National Academy of Sciences*, 87(15):5832–5836, 1990.

[158] Kazunori Yoshida and Hiroshi Oka. Topographical distribution of septohippocampal projections demonstrated by the pha-l immunohistochemical method in rats. *Neuroscience letters*, 113(3): 247–252, 1990.

Colophon

This thesis was typeset using LaTeX, originally developed by Leslie Lamport and based on Donald Knuth's TeXand modified by the author (Negar Nikbakht). The sidenotes are inspired by the design of Tufte-LaTeX. The body text is set in 11 point Arno Pro, designed by Robert Slimbach in the style of book types from the Aldine Press in Venice, and issued by Adobe in 2007. A template, which can be used to format a PhD thesis with this look and feel, has been released under the permissive MIT (x11) license, and can be found online at github.com/suchow/.